Roles of aquaporin-4 and Kir4.1 in brain water and potassium homeostasis: lessons from knockout mice

by

Nadia Nabil Haj-Yasein

Thesis for the degree of Philosophiae Doctor (PhD)

Centre for Molecular Biology and Neuroscience

&

Centre for Molecular Medicine Norway

University of Oslo

Principle supervisor:

Dr. Erlend A. Nagelhus

Co-supervisors:

Dr. Øivind Hvalby

Dr. Vidar Jensen

Series of dissertations submitted to the
Faculty of Medicine, University of Oslo
No. 1268

ISBN 978-82-8264-342-9

Cover: Inger Sandved Anfinsen.
Printed in Norway: AIT Oslo AS.

Produced in co-operation with Unipub.
The thesis is produced by Unipub merely in connection with the
thesis defence. Kindly direct all inquiries regarding the thesis to the copyright
holder or the unit which grants the doctorate.

TABLE OF CONTENTS

ACKNOWLEDGEMENTS

First and foremost I would like to thank my parents Nabil and Naela, my brothers Nader and Nasser, my sisters Nada and Nebal, who through my childhood and study career had always encouraged me to follow my heart and inquisitive mind in any direction this took me. I am deeply and forever indebted to my parents for their love, support and encouragement throughout my entire life.

I would like to express my gratitude to my supervisor Dr. Erlend A. Nagelhus for being an outstanding advisor. His constant encouragement, support, patience, flexibility, genuine caring and concern, and faith in me during the PhD period, enabled me to complete this thesis. My sincere appreciation and gratitude also go to Prof. Ole Petter Ottersen for his invaluable support and encouragement. It is a pleasure to thank those who made this thesis possible, especially my excellent co-supervisors Dr. Øivind Hvalby and Dr. Vidar Jensen for all the teaching, support, assistance, fruitful discussions and the joyful moments we spent together in the lab. Working with them has been a great pleasure for me.

My deepest gratitude to our collaborators, especially to Prof. Kai Kaila and Juha Voipio at the University of Helsinki and Prof. Maiken Nedergaard at the University of Rochester, New York.

Special thanks to: Bjørg Riber, Karen Marie Gujord, Jorunn Knutsen, Carina Knudsen and Gunnar Lothe, I am so grateful for your help all these years. To Johannes Helm, thanks to you for being available at any time.
My co-authors, George Andreas, Rune, Martina, Anna and John thank you for the nice teamwork.
Also thanks to my colleagues for their help and assistance. In particular I would like to thank Katja Stahl, Gry Vindedal, Laura Maria Azzura, Hanna Ahlgren and Cecilie Bugge for being such great colleagues and friends. I also acknowledge Professor Eric Rinvik, Dr.Reidun Torp, Dr.Mahmood Amiry-Moghaddam, and Dr. Lasse Ormel.

Special heartfelt thanks to Kristine Knudsen for caring all the way, being a great support during the hard times, in addition to the administrative help.

Maria Niki Mylonakou, you have been more than a colleague for me, you are my third sister. Thank you for all the time we spent together. Maria you are a wonderful and generous friend.

Øystein Grønning and Marit Unstad, thank you for being my family in Oslo.
Ayman AlAzraq, I would like to thank you for the help during the years of my PhD.

I would like to express my gratitude for the fundings I got to complete this PhD thesis, first from The Marie Curie Training Network CORTEX (Cooperation in Research and Training for European Excellence in the Neurosciences), thereafter from the Research Council of Norway (NevroNor grant to E.A.N.) and the Center for Molecular Medicine Norway (NCMM), Nordic EMBL Partnership, University of Oslo.

The present work was carried out at the Center for Molecular Biology and Neuroscience (CMBN) and at the Department of Anatomy, Institute of Basic Medical Sciences and NCMM, University of Oslo.

ABBREVIATIONS

AQP aquaporin

Aqp4 aquaporin-4 mouse gene

BBB blood-brain barrier

CA1 cornu ammonis

CNS central nervous system

CSF cerebrospinal fluid

DAPC dystrophin associated protein complex

Dp71 short dystrophin isoform (71kDa)

DRE delayed response enhancement

EAAT excitatory amino-acid transporter (glutamate transporter)

ECS extracellular space

GABA gamma aminobutyric acid

GAT gamma aminobutyric acid (GABA) transporter

GFAP glial fibrillary acidic protein

GLUT1 glucose transporter 1

HRP horse radish peroxidase

Hz hertz

ISM ion sensitive microelectrode

kDa kilodalton

Kir inwardly rectifying potassium channel

KCC potassium-chloride cotransporter

KCNJ10 gene encoding Kir4.1

LTP long term potentiation

MCT monocarboxylate transporter

NKCC1 sodium-potassium-chloride (Na-K-Cl) cotransporter

OAP orthogonal arrays of intramembranous particles

PDZ is a common structural domain found in some proteins

RVD	regulatory volume decrease
TMA^+	tetramethylammonium

LIST OF PAPERS INCLUDED IN THE THESIS

Paper I: **Nadia Nabil Haj-Yasein**,Vidar Jensen, Gry Fluge Vindedal, Georg Andreas Gundersen Arne Klungland, Ole Petter Ottersen, Øivind Hvalby, and Erlend Arnulf Nagelhus. Evidence that compromised K+ spatial buffering contributes to the epileptogenic effect of mutations in the human Kir4.1 gene (KCNJ10). Glia 59(11):1635-42. [Epub July 11, 2011]

Paper II: **Nadia Nabil Haj-Yasein**, Vidar Jensen, Ivar Østby, Stig Omholt, Juha Voipio, Kai Kaila, Ole Petter Ottersen, Øivind Hvalby, and Erlend A. Nagelhus.
Aquaporin-4 regulates extracellular space volume dynamics during high-frequency synaptic stimulation: a gene deletion study in mouse hippocampus. Submitted.

Paper III: Martine Eilert-Olsen, **Nadia Nabil Haj-Yasein**, Gry Fluge Vindedal, Rune Enger, Georg Andreas Gundersen, Pétur Henry Petersen, Finn-Mogens S. Haug, Øivind Skare, Marvin E. Adams, Stanley C. Froehner, John Michael Burkhardt, Anna E. Thoren, and Erlend A. Nagelhus. Deletion of aquaporin-4 changes the perivascular glial protein scaffold without disrupting the endothelial barrier. Glia, in press.

Paper IV: **Nadia Nabil Haj-Yasein**, Gry Fluge Vindedal, Martine Eilert-Olsen, Georg Andreas Gundersen, Øivind Skare, Petter Laake, Arne Klungland, Anna E. Thoren, John Michael Burkhardt, Ole Petter Ottersen, and Erlend A. Nagelhus. Glial-conditional deletion of aquaporin-4 (*Aqp4*) reduces blood-brain water uptake and confers barrier function on perivascular astrocyte endfeet. Proceedings of the National Academy of Sciences U.S.A. 108 (43):17815-20. Epub 2011 Oct 11.

INTRODUCTION

Homeostasis, the ability to maintain stability and equilibrium of the internal environment in the face of external changes, is a prerequisite for life. Notably, control of temperature and hydration is critical for body function, as is maintenance of cellular levels of water, ions, glucose, and oxygen (Wynsberghe Donna 1995; Boron Walter 2005) .

Water is distributed in intra- and extracellular spaces with a ratio of 55:45. The intra- and extracellular fluids are separated by the cell membrane.

Ion and water homeostasis is maintained by transporters and channels localized to the plasma membrane (Cogan 1991; Simard and Nedergaard 2004; Boron Walter 2005). Dysfunction or lack of these membrane proteins may disrupt ion- and water homeostasis and cause disease. An example is ischemic brain edema.

Water crosses cell membranes by different means: 1) by slow diffusion through the lipid bilayer, 2) through cotransporters and uniporters, and 3) through aquaporin water channels (Fig. 1) (Agre 2004; MacAulay, Hamann et al. 2004). Water transport is generally considered to be passive, i. e. driven by hydrostatic and osmotic gradients. Thus, transport of water is intimately linked to transport of solutes. Water transport by cotransporters constitutes a special case, as some studies indicate that these are capable of moving water even against osmotic gradients. Such an active transport of water is thought to rely on conformational changes during the transport cycle, causing release of water molecules that are forming a shell around the transported solutes. Up to 590 water molecules can follow the solutes during each transport cycle (MacAulay and Zeuthen 2010).

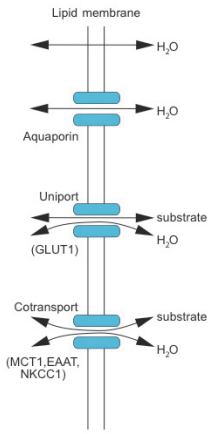

Figure 1. Moods of water transport through the cell membrane

Cotransporters are highly expressed in the brain. The main cotransporters in neuropil are KCC (K^+-Cl^-), NKCC1 (Na^+-K^+-$2Cl^-$), MCT (H^+-lactate), GAT (Na^+-GABA), and EAAT (Na^+-

glutamate). KCC is an electroneutral cotransporter for K^+ and Cl^-. In many cell types it is involved in regulatory volume decrease (RVD) and is colocalized with the Na^+/K^+-ATPase. NKCC1 is also electroneutral and transports Na^+ and K^+ together with 2 Cl^-. The MCTs transport protons and monocarboxylates, notably lactate, and are particularly enriched in capillary endothelial cells. The EAATs are electrogenic and couple glutamate transport with the transport of Na^+, H^+ and K^+. Likewise, GATs are electrogenic and transport GABA, Na^+ and Cl^- (MacAulay, Hamann et al. 2004). The latter two are particularly enriched in glial membranes ensheating synapses (Danbolt, Chaudhry et al. 1998).

The glucose transporter GLUT1 is abundant in the central nervous system (CNS). It is expressed at high levels in capillaries and at lower levels in glial membranes (Bergersen, Johannsson et al. 1999). Since GLUT1 is permeable for water it could play a significant role in water transport across the blood-brain barrier.

Aquaporin water channels are integral membrane proteins that mediate rapid transport of water with high selectivity (King, Kozono et al. 2004). The first aquaporin was discovered in 1992 by Peter Agre's group and was named aquaporin-1 (AQP1) (Preston, Carroll et al. 1992). For the discovery of aquaporins Agre was awarded the Nobel Prize in Chemistry in 2003.

Aquaporins are ubiquitously expressed and hitherto 13 mammalian aquaporins have been identified. Aquaporins are divided into 3 subgroups:

1) aquaporins permeable only to water: AQP0, AQP1, AQP2, AQP4, AQP5, AQP6.
2) aquaglyceroporins permeable to water, glycerol and urea: AQP3, AQP7, AQP8, AQP9.
3) Aquaporins with unknown substrate specificity: AQP10-12.
   (Badaut, Lasbennes et al. 2002; Gomes, Agasse et al. 2009; Ishibashi, Koike et al. 2009; Badaut 2010).

Aquaporins in the brain

AQP1, AQP4, and AQP9 are the most prevalent aquaporins in the rodent brain (Badaut, Lasbennes et al. 2002; Amiry-Moghaddam and Ottersen 2003). AQP1 is expressed in choroid

plexus epithelial cells and is involved in the production of cerebrospinal fluid (CSF) (Nielsen, Smith et al. 1993; Oshio, Watanabe et al. 2005). AQP4 is expressed in astrocytes and ependymal cells (Frigeri, Gropper et al. 1995; Nielsen, Nagelhus et al. 1997). Conflicting data exist on the distribution of AQP9. Elkjær et al. reported that AQP9 is expressed in tanycytes surrounding the cerebral ventricles, but not in neurons and astrocytes (Elkjaer, Vajda et al. 2000). However, Zelenina et al. reported that AQP9 is expressed in astrocytes, endothelial cells of the subpial blood vessels, and in a subpopulation of neurons (Zelenina 2010). Amiry-Moghaddam et al. reported AQP9 expression in mitochondria of some neurons and astrocytes (Amiry-Moghaddam, Lindland et al. 2005). Other aquaporins are expressed at very low levels in brain.

This thesis focuses on AQP4 and associated molecules in the glial cell membrane. AQP4 has a polarized distribution and is concentrated at the interface between brain tissue and the main fluid compartments of the CNS (Nielsen, Nagelhus et al. 1997; Nagelhus, Veruki et al. 1998) (Fig. 2). Notably, AQP4 expression is tenfold higher in glial endfoot membranes abutting on blood vessels and facing the pial surface, than in glial membranes ensheating synapses (Nielsen, Nagelhus et al. 1997; Nagelhus, Mathiisen et al. 2004). AQP4 is not expressed in neurons, oligodendrocytes or microglia (Nielsen, Nagelhus et al. 1997; Amiry-Moghaddam and Ottersen 2003). Expression of AQP4 in brain is very low at birth, but increases in the second and third postnatal week, concomitant with the maturation of astrocytes (Wen, Nagelhus et al. 1999).

AQP4 has six transmembrane domains and both the amino (N)- and the carboxyl (C)-termini are intracellular. The protein exists in two major isoforms, as the AQP4 gene has two transcriptional initiation sites. Isoform M1 has 323 amino acids and M23 has 301 amino acids (Jung, Bhat et al. 1994). The molecular weight of the isoforms is 34kDa and 32kDa, respectively. Cerebral expression of M23 is at least 3 times that of M1 (Neely, Christensen et al. 1999).

A general feature of aquaporins is that they form tetramers in the cell membrane (King, Kozono et al. 2004). AQP4 is unusual in that the tetramers cluster in large assemblies termed orthogonal arrays of intramembranous particles (OAPs) or square arrays (Rash, Yasumura et al.

1998; Furman, Gorelick-Feldman et al. 2003). OAPs were discovered by freeze-fracture electron microscopy several decades ago, but their molecular identity remained unknown for many years (Wolburg 1995). A breakthrough came with the discovery that OAPs are absent in AQP4 knockout mice (Verbavatz, Ma et al. 1997). Biochemical studies have shown that the M23 isoform is critical for the formation of large OAPs in endfeet, while the M1 isoform forms smaller units (Furman, Gorelick-Feldman et al. 2003; Nicchia, Rossi et al. 2008; Nicchia, Rossi et al. 2010).

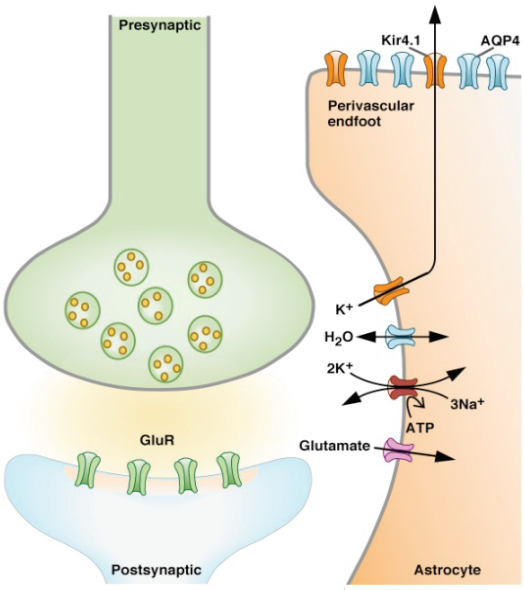

Figure 2. Astrocytes are considered important for the regulation of $[K^+]_o$ and $[glutamate]_o$ in the synaptic cleft. Astrocytic membranes ensheating synapses are equipped with AQP4, Kir4.1 potassium channels, Na^+/K^+-ATPase and glutamate transporters. Perivascular astrocytic endfoot membranes are abundant in AQP4 and also express Kir4.1. Modified from Amiry-Moghaddam & Ottersen, 2003, with permission.

Astrocytes

In the human cortex there are 1.4 astrocytes for each neuron (Bass, Hess et al. 1971). The major types of glial cells are oligodendrocytes, microglia, ependymocytes and astrocytes (Krawczyk and Jaworska-Adamu 2010). The term astrocyte was introduced in 1893 by Michael von Lenhossek to describe the star-shaped cells seen with silver staining techniques (Garcia-Marin, Garcia-Lopez et al. 2007). A similar shape is evident in immunohistochemical sections when using antibodies against the glial fibrillary acidic protein (GFAP) (Simard, Arcuino et al. 2003). However, imaging of astrocytes filled with dye through patch-pipettes reveals a much more complex and bushy architecture (Bushong, Martone et al. 2002). The processes that ensheat the synapses are thin and leaflet-like, as confirmed by electron microscopy (Nielsen, Nagelhus et al. 1997). Astrocytic endfeet abutting blood vessels or facing the pial surface also have a complex morphology, with thin interdigitating processes (Nielsen, Nagelhus et al. 1997; Simard, Arcuino et al. 2003). In mammals astrocytes are spatially organized into minimally overlapping domains (Oberheim, Wang et al. 2006; Wilhelmsson, Bushong et al. 2006).

The exact roles of the astrocytes in the central nervous system are still not fully understood. Despite the fact that the word glia is derived from the greek word for glue, the functions of glial cells extend far beyond adhesion and support (Nedergaard, Ransom et al. 2003). Astrocytes maintain homeostasis through uptake of neurotransmitters and ions released during neuronal activity, detoxification of ammonium, and regulation of extracellular pH. Recent studies suggest that astrocytes are actively participating in synaptic transmission, hence the term tripartite synapse (Haydon and Carmignoto 2006). Notably, astrocytes sense synaptic activity, respond with increases in intracellular Ca^{2+} concentration, and release signaling molecules ("gliotransmitters") that in turn influence pre- and/or postsynaptic neurons (Kimelberg and Nedergaard 2010). Astrocytes also play a role in pathological conditions such as cytotoxic edema, glioma formation, and neuroinflammation (Ransom, Behar et al. 2003; Simard and Nedergaard 2004; Pekny, Wilhelmsson et al. 2007).

Anchoring of AQP4

The clustering of AQP4 in glial endfoot membranes depends on dystrophin and the dystrophin associated protein complex (DAPC), in particular α-syntrophin (Frigeri, Nicchia et al. 2001; Neely, Amiry-Moghaddam et al. 2001) (Fig.3). The dystrophin gene is the largest gene in the human genome, making up 1.5% of the X chromosome. Most of the gene is composed of introns although it contains as many as 86 exons. There are several long and short isoforms of this protein. Dystrophin is expressed in skeletal muscle, cardiac muscle, and brain. Mutations in the dystrophin gene can lead to variety of muscular dysfunction disorders – including muscular dystrophy - and some of these disorders are also associated with neurological symptoms (Muntoni, Torelli et al. 2003). It is the short dystrophin isoform Dp71 (71kDa) that is expressed in astrocytes (Lumeng, Hauser et al. 1999; Muntoni, Torelli et al. 2003).

Dystrophin (or its autosomal homologue utrophin) assembles with five proteins, each having isoforms; dystroglycan, syntrophin, dystrobrevin, sarcoglycan and sarcospan. It has been reported that syntrophin requires dystrophin or utrophin to assemble the DAPC and to target it to the membrane. Notably, the cytoskeleton and extracellular matrix connect through the DAPC (Vajda, Pedersen et al. 2002).

The syntrophin family is composed of five proteins (α, β1, β2, γ1, γ2). All syntrophin isoforms express two PDZ domains and a unique C-terminal region which can bind to different proteins so as to generate functional protein complexes (Adams, Mueller et al. 2001; Neely, Amiry-Moghaddam et al. 2001). AQP4 has a Ser-Ser-Val (S-S-V) sequence on the C-terminus. This sequence has the capacity to bind to a PDZ domain of syntrophin. Deletion of α-syntrophin reduces the perivascular and subpial pool of AQP4, pointing to a role of α-syntrophin in the anchoring of AQP4 (Neely, Amiry-Moghaddam et al. 2001; Amiry-Moghaddam, Otsuka et al. 2003; Amiry-Moghaddam, Williamson et al. 2003).

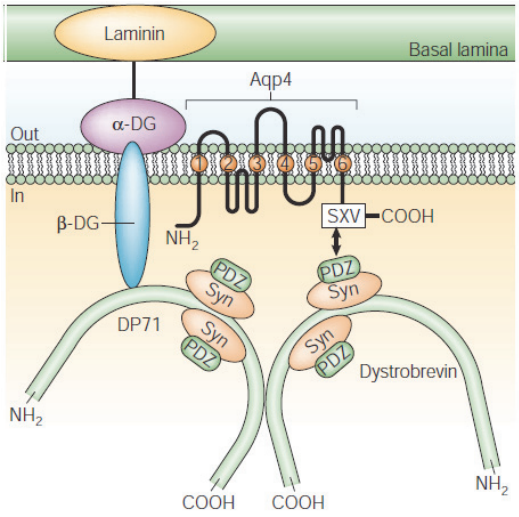

Figure 3. The dystrophin-associated protein complex (DAP) is a large membrane assembly that connects the cytoskeleton to the extracellular matrix. The short dystrophin isoform Dp71 binds the transmembrane protein β-dystroglycan (β-DG), which connects to the laminin/agrin-binding protein α-DG. On the cytoplasmic side of the complex, dystrophin binds to α-dystrobrevin. Each dystrophin and α-dystrobrevin molecule can bind up to two syntrophins. Syntrophins contain a PDZ domain that serves as an adaptor for the recruitment of membrane channels. α-syntrophin is the main syntrophin expressed in astrocytic endfeet and is thought to be responsible for the clustering of AQP4 in endfoot membranes, through an indirect interaction of the AQP4 sequence Ser-X-Val with its PDZ domain (Figure and modified legend are from Amiry-Moghaddam and Ottersen, 2003, with permission).

Kir4.1

The inwardly rectifying potassium channel Kir4.1 is expressed in glia and is colocalized with AQP4 in glial endfoot membranes (Nagelhus, Horio et al. 1999; Amiry-Moghaddam, Williamson et al. 2003). In α-syn$^{-/-}$ mice – in which perivascular AQP4 expression is significantly reduced – expression of Kir4.1 in glial endfeet in retina and hippocampus is not significantly reduced (Amiry-Moghaddam, Williamson et al. 2003; Puwarawuttipanit, Bragg et al. 2006). The latter study indicates that α-syntrophin is not the primary anchoring protein for Kir4.1. However, a biochemical study indicates that Kir4.1 associates with the DAPC via α-syntrophin in brain (Connors, Adams et al. 2004). The reason for this discrepancy is unknown.

The colocalization of AQP4 and Kir4.1 in retina and brain led to the assumption that these proteins are functionally coupled. Notably, it was proposed that K^+ clearance is coupled

with water flux through AQP4 (Nielsen, Nagelhus et al. 1997; Nagelhus, Horio et al. 1999; Amiry-Moghaddam, Williamson et al. 2003). In support of this hypothesis deletion of α-syntrophin delayed K^+ clearance following high frequency activation of excitatory pathways in acute hippocampal slices (Amiry-Moghaddam, Williamson et al. 2003). Moreover, seizure severity was increased in these mutant mice. Later it was shown that deletion of *Aqp4* also delayed K^+ clearance (Binder, Yao et al. 2006). Somewhat surprising, a higher seizure threshold was found in *Aqp4*$^{-/-}$ mice, but this probably reflects widening of the extracellular space (ECS) in these mice (Yao, Hrabetova et al. 2008). Whether and how AQP4 and Kir4.1 interact remains controversial. A recent study concluded that Kir4.1 is sensitive to volume changes and hence influenced by AQP4 (Soe, Macaulay et al. 2009). On the other hand, Müller cells obtained from *Aqp4*$^{-/-}$ mice retained their ability to handle K^+ (Ruiz-Ederra, Zhang et al. 2007).

Regulation of extracellular [K^+] during synaptic activity

It is well known that K^+ is released to the extracellular space from active synapses. Clearance of K^+ is critical as K^+ accumulation in the extracellular space will lead to neuronal depolarization and cause epileptiform discharges (Higashi, Fujita et al. 2001; Amiry-Moghaddam, Williamson et al. 2003). Extracellular K^+ concentration in brain is ~3 mM. Synaptic stimulation increases the K^+ concentration until it reaches a plateau (ceiling level) at about 10-12 mM. This ceiling level is exceeded only in pathophysiological conditions such as cortical spreading depression (Kofuji and Newman 2004).

A role for glial cells in K^+ clearance from activated synapses was suggested by Orkand et al. (1966). Two decades later Eric Newman and colleagues showed that retinal Müller cells cleared excess K^+ by spatial redistribution (Newman, Frambach et al. 1984). The clustering of K^+ channels in glial endfeet caused excess K^+ to be directed to specific compartments (i.e. the perivascular and vitreous spaces), and hence the term K^+ siphoning was introduced (Newman, Frambach et al. 1984; Karwoski, Lu et al. 1989). Spatial redistribution of K^+ was ascribed to inwardly rectifying channels, but the exact identify of the channels was unknown for many years.

The discovery of Kir4.1 channels in glial endfeet (Nagelhus, Horio et al. 1999) resolved the molecular identity of the channels responsible for K^+ siphoning.

Glial cells are considered to play an important role in extracellular K^+ homeostasis. Removal of K^+ from the extracellular space occurs by net uptake and K^+ spatial buffering (Fig. 4).

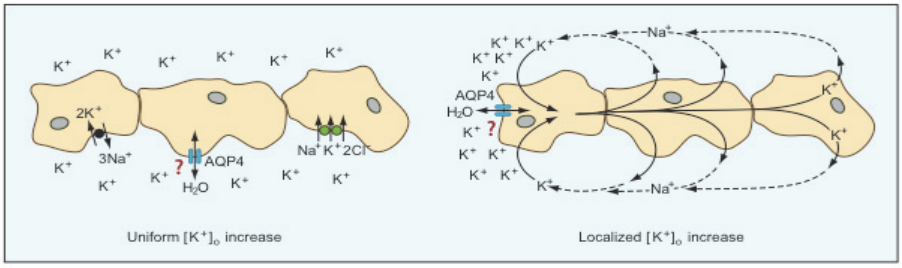

Figure 4. Principal modes of K^+ clearance by glial cells.

In K^+ net uptake, K^+ accumulates in glial cells mainly due to the activity of the Na^+,K^+–ATPase or the Na^+,K^+,Cl^- cotransporter (Orkand 1986; Kofuji and Newman 2004). Uptake of K^+ and Cl^- through separate channels is also possible.

In K^+ spatial buffering, K^+ is redistributed from an area with high $[K^+]_o$ to an area with lower $[K^+]_o$. The K^+ fluxes through the syncytium of gap junction-coupled astrocytes. The driving force for K^+ fluxes is the difference between the local K^+ equilibrium potential (E_k) and the syncytium membrane potential (Vm). A special form of spatial buffering is K^+ siphoning, where K^+ is directed to blood vessels or the surface of nervous tissue through K^+ channels clustered in glial endfeet (cf. Fig. 2).

Brain edema

Brain edema is defined as accumulation of excess water in the intracellular and/or extracellular spaces of the brain. In the 1960s Igor Klatzo suggested to classify brain swelling into cytotoxic

edema and vasogenic edema. Later hydrocephalic edema was added as a major edema type (Papadopoulos and Verkman 2007). Cytotoxic edema is characterized by cellular swelling and is typically seen in hyponatremia and the early phase of cerebral ischemia. In the latter situation transmembrane ionic gradients and cell volume are disturbed due to energy failure. Vasogenic edema is characterized by extracellular fluid accumulation due to opening of the blood brain barrier (Papadopoulos and Verkman 2007). It is typically seen in brain injury and inflammation or is associated with brain tumors.

The seminal discovery that *Aqp4* knockout reduced brain edema in experimental stroke and hyponatremia suggested that AQP4 regulates water transport between blood and brain (Manley, Fujimura et al. 2000). Similar data obtained in animal models with targeted deletion of the perivascular pool of AQP4 confirmed this concept (Vajda, Pedersen et al. 2002; Amiry-Moghaddam, Otsuka et al. 2003). Since it is well documented that AQP4 aggravates cytotoxic brain edema, AQP4 is now regarded as a promising target for new therapies in edematous states (Verkman 2009). However, whereas *Aqp4* deletion reduced cytotoxic brain swelling it proved to have the opposite effect on vasogenic brain edema (Papadopoulos, Manley et al. 2004). Thus, in situations where the blood brain barrier (BBB) is disrupted and there is extracellular fluid accumulation, AQP4 function should be enhanced rather than inhibited. Our limited knowledge on the precise roles of AQP4 in various disease states and in physiology are obviously calls for further investigations.

Blood-brain barrier

In 1885 Paul Ehrlich injected a dye intravenously and noted that all organs were colored except the brain and the spinal cord. Almost 30 years later Edwin Goldmann, one of Ehrlich's students, observed that brain tissue was stained if the same dye was injected into the cerebrospinal fluid (Wolburg, Noell et al. 2009; Cardoso, Brites et al. 2010). These observations led to the conclusion that there must be a blood-brain barrier (BBB)(Wolburg, Noell et al. 2009; Abbott, Patabendige et al. 2010; Cardoso, Brites et al. 2010). After the advent of the electron

microscope it became clear that endothelial tight junctions constituted an essential morphological substrate for the barrier (Reese and Karnovsky 1967).

The BBB has various functions, including:

1) regulation and maintenance of ion and neurotransmitter homeostasis in the CNS
2) restriction of fluid movement between the brain and blood
3) protection of the CNS from neurotoxins
4) controlling permeability of macromolecules and solutes
5) supplying the brain with nutrients
6) removing waste and harmful products

(Abbott, Ronnback et al. 2006; Abbott, Patabendige et al. 2010; Cardoso, Brites et al. 2010).

The BBB has many components; the main and essential one is the endothelial cell layer. In addition, pericytes, astrocytes, microglia and the basal lamina are also important parts of the BBB (Wolburg, Noell et al. 2009; Cardoso, Brites et al. 2010).

Tight junctions between the endothelial cells reduce the movement of solutes through the intercellular space, and thus force substances to use transcellular routes in order to pass the BBB (Abbott, Ronnback et al. 2006; Saunders, Ek et al. 2008). Gases such as O_2, CO_2 and small lipophilic molecule (such as barbiturates and ethanol) can diffuse quite easily through the lipid cell membrane. Luminal and abluminal membranes have transporters that regulate movement of small hydrophilic molecules and discharge toxic material. Another feature of brain endothelial cells is their lower capability for endocytosis compared to endothelium in extracerebral organs (Abbott, Ronnback et al. 2006).

Astrocytes are considered to be important for the integrity of the BBB, as loss of astrocytic proteins, notably dystrophin, is associated with BBB dysfunction (Nico, Paola Nicchia et al. 2004).

CNS fluid dynamics at the macroscopic level

CNS water is distributed in different compartments: blood, cerebrospinal fluid (CSF), interstitial fluid, and intracellular fluid. It moves according to hydrostatic and osmotic gradients (Papadopoulos and Verkman 2007), but the precise routes of the fluid movements are still poorly characterized.

CSF is a clear fluid that is localized within and surrounding the CNS. It is acting both as a fluid cushion and drainage route for metabolic products (Moody 2006). Also, it provides a specialized extracellular environment where transport of nutrients, peptides, and hormones can take place (Oshio, Watanabe et al. 2005).

The major production of CSF occurs in the different choroid plexi localized to the ventricles. The fluid enters the subarachnoid space from the ventricle system through three holes in the ceiling of the fourth ventricle and is drained out to the sinus venosus through the arachnoid granulations. From the subarachnoid space CSF will spread over the brain and the spinal cord. The production of brain interstitial fluid is less clear, but likely derives both from blood as well as CSF within ventricles(Kimelberg 2004).

Water within the brain parenchyma can be cleared via three major routes:

1) Across the BBB to the blood stream
2) Across the ependymal cells to the ventricles
3) Across the pial surface to the subarachnoid space

The three routes are lined up by glia (astrocytic endfeet, ependymal cells) that express AQP4 (Papadopoulos and Verkman 2007).

Brain fluid dynamics at the synaptic level

Reversible changes in the size of the intracellular and extracellular spaces occur during neuronal activation. Following stimulation, shrinkage of the ECS and swelling of the cellular compartment are observed (Sykova and Nicholson 2008). The dynamic volume changes are thought to reflect

water redistribution due to ion fluxes between the respective compartments. The exact contribution of the various channels and transporters (cf Fig. 2) probably depends on the intensity of stimulation and the region studied. Very few studies have attempted to resolve these issues.

Animal models

Gene knockout animals have greatly increased our knowledge of the function of the respective gene products (Gaveriaux-Ruff and Kieffer 2007; Bockamp, Sprengel et al. 2008). A potential drawback of the conventional knockout approach - gene deletion at a one cell stage - is the lethal phenotype when the deleted gene is important for the development and survival (Gaveriaux-Ruff and Kieffer 2007). To overcome this problem conditional knockout models have become more popular, especially the Cre mediated LoxP-specific recombination (van der Neut 1997; Gaveriaux-Ruff and Kieffer 2007; Bockamp, Sprengel et al. 2008). Cre recombinase is encoded by the E. Coli bacteriophage P1 and has the ability to do induce recombination between two recognition sites called LoxP sites (van der Neut 1997; Nagy 2000; Gaveriaux-Ruff and Kieffer 2007; Morozov 2008). The strategy to generate a conditional knockout mouse using the Cre loxP approach involves three steps:

1) Insertion of LoxP sites around the gene of interest or the essential exons by homologous recombination in embryonic stem cells. Gene function should not be influenced by the LoxP sites, as they are localized to introns.

2) Generation of a transgenic mouse line with the Cre recombinase gene under control of a cell type specific promoter (many such Cre lines are commercially available). In some strains the Cre recombinase can be turned on by the use of tetracyclin or tamoxifen.

3) Breeding of floxed mice with mice carrying the Cre gene and intercrossing of offspring. Mice homozygous for the floxed allele and positive for Cre recombinase will undergo irreversible excision of the gene located between the loxP sites. The recombination will only take place in cells expressing the promoter that drives Cre (Lodish H 2000; Gaveriaux-Ruff and Kieffer 2007).

AIMS OF THE THESIS

The overriding goal of the present work was to identify functional roles of the two astrocytic proteins, Kir4.1 and AQP4. These proteins are considered essential for ion and water homeostasis in brain and are colocalized at the cellular and subcellular levels. A number of genetically manipulated mouse lines, one generated specifically for this work, were used to delineate molecular function (Fig.5).

In paper I, using a glia specific Kir4.1 knockout, we aimed to establish whether astrocytic Kir4.1 mediates K^+ spatial buffering in brain. If so, this would provide a mechanistic underpinning of the epilepsy phenotype associated with mutations in KCNJ10 – the gene encoding Kir4.1.

The fine astrocytic processes ensheathing excitatory synapses in brain might not only be involved in K^+ homeostasis (an issue addressed in Paper I), but also in the regulation of extracellular volume. Specifically, we asked whether deletion of the *Aqp4* gene would affect extracellular volume dynamics following high frequency stimulation of excitatory pathways. A global *Aqp4*$^{-/-}$ mouse line was used for this purpose.

Moving from the synaptic region to the brain-blood interface, the aims of papers III and IV were to resolve the roles of AQP4 in regulating barrier function and water transport between blood and brain.

In paper III, we asked whether deletion of the *Aqp4* gene led to changes in the expression of other proteins at the gliovascular junction – including dystrophin and dystrophin associated proteins, and proteins known to be involved in the endothelial barrier (occludins and claudins). We also performed tracer studies to resolve whether *Aqp4* deletion interfered with the endothelial barrier function.

In paper IV we sought to clarify whether astrocytes regulate water transport at the blood-brain interface. A glial conditional *Aqp4* knockout mouse was engineered for this purpose. As a secondary aim we tested whether loss of astrocytic AQP4 interfered with the brain water resorption that normally occurs in the first postnatal weeks.

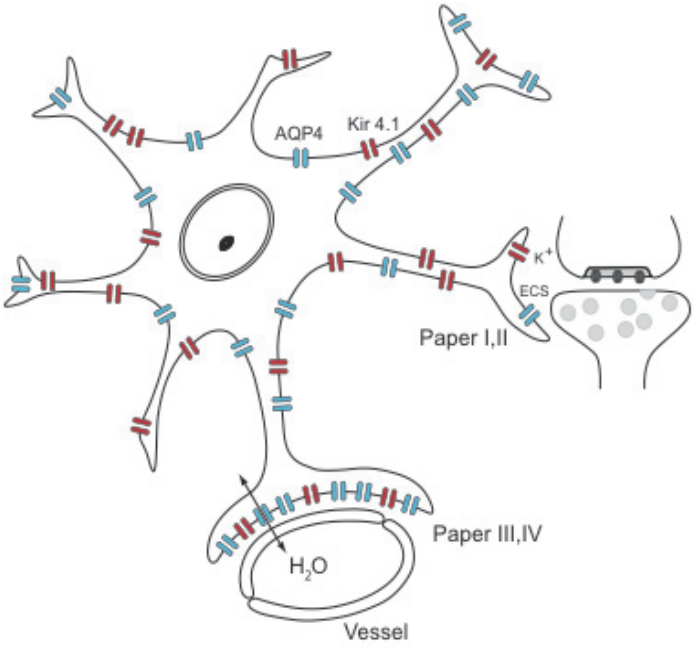

Figure 5. The papers included in the thesis focus on AQP4 and Kir4.1 in glial processes around synapses (Paper I & II) and at the blood-brain interface (Paper III & IV).

RESULTS OF THE INDIVIDUAL PAPERS

Paper I: Evidence that compromised K^+ spatial buffering contributes to the epileptogenic effect of mutations in the human Kir4.1 gene (KCNJ10)

Immunofluorecence, immunogold cytochemistry and immunoblotting showed that AQP4 expression was not significantly affected by glial-conditional deletion of Kir4.1. Immunofluorescence confirmed Kir4.1 labeling of astrocytes in the stratum radiatum of the hippocampal cornu ammonis (CA1) region where the K^+-selective electrodes were placed. Conditional deletion of Kir4.1 delayed clearance of extracellular K^+ following 20 Hz stimulation of the afferent fibers, and also increased the $[K^+]_o$ undershoot after multiple stimulation trains. Extracellular volume changes, assessed by ion-sensitive microelectrodes (ISMs) and the membrane-impermeable cation tetramethylammonium (TMA^+), did not differ between the genotypes.

We concluded that astrocytic Kir4.1 channels mediate K^+ spatial buffering in brain and that compromised K^+ spatial buffering could contribute to the epileptogenic effect of KCNJ10 mutations.

Paper II: Aquaporin-4 regulates extracellular space volume dynamics during high-frequency synaptic stimulation: a gene deletion study in mouse hippocampus

Immunofluorescence and immunogold cytochemistry revealed AQP4 labeling of astrocytic processes in the stratum radiatum and stratum pyramidale of the hippocampal CA1 region. Global deletion of *Aqp4* did not change the morphology of astrocytic processes in hippocampus. ECS shrinkage during 20 Hz stimulation of the Schaffer collateral/commissural pathway was significantly increased in *Aqp4*$^{-/-}$ mice compared to the wild-type. In both genotypes the ECS shrinkage was more pronounced in the stratum pyramidale compared to the stratum radiatum.

Excitatory synaptic transmission, frequency facilitation, delayed response enhancement (DRE) and long term potentiation (LTP) were similar in the two genotypes.

We concluded that AQP4 regulates ECS volume dynamics during synaptic activity and serves to counteract activity-dependent ECS shrinkage. The pronounced ECS shrinkage in the stratum pyramidale most likely reflects as expansion of the neuronal compartment.

Paper III: Deletion of aquaporin-4 changes the perivascular glial protein scaffold without disrupting the endothelial barrier.

Using quantitative immunogold cytochemistry and immunoflurescence we showed that perivascular α-syntrophin labeling was reduced in *Aqp4*$^{-/-}$ mice. Immunofluorescence also revealed that perivascular dystrophin was also reduced in mutant mice. In contrast, *Aqp4* deletion did not change the ultrastructure of astrocytic endfeet or endothelial cells. Notably, tight junctions appeared normal in *Aqp4*$^{-/-}$ mice.

Qualitative and quantitative assessment of the blood-brain barrier permeability using horseradish peroxidase (HRP) and Evans blue albumin dye showed no differences between genotypes.

We concluded that global deletion of *Aqp4* changes the perivascular glial protein scaffold without disrupting the endothelial barrier.

Paper IV: Glial-conditional deletion of aquaporin-4 (*Aqp4*) reduces blood-brain water uptake and confers barrier function on perivascular astrocyte endfeet.

The strategy to use the GFAP promoter to drive recombination in glia resulted in a complete loss of glial AQP4 in the mutants, as measured by immunofluorescence, and quantitative immunoblotting. Glial-conditional *Aqp4*$^{-/-}$ mice displayed normal AQP4 expression in kidney and muscle. Quantitative immunogold cytochemistry of wild-type, glial-conditional, and global

Aqp4$^{-/-}$ mice revealed that endothelial membranes are devoid of AQP4 labeling. Having resolved the controversy regarding the endothelial expression of AQP4, we went on to study whether the glial pool of AQP4 regulates blood-brain water uptake. Indeed, systemic hypo-osmotic stress caused significantly less water accumulation in the brain of glial-conditional *Aqp4* knockout mice than in control animals. We also found that basal brain water content was elevated in glial-conditional and global *Aqp4*$^{-/-}$ mice. This effect was evident already at postnatal day 8, suggesting that AQP4 facilitates water resorption in early postnatal life. The permeability of the blood-brain barrier was assessed by Evans blue dye extravasation and did not differ between glial-conditional and control mice.

We concluded that the blood-brain barrier is more complex than anticipated and that the glial covering of brain microvessels in certain circumstances acts as a functional barrier to water movement. Moreover, our data do not support the hypothesis that AQP4 is expressed in endothelial cells.

DISCUSSION

Astrocytes have enjoyed a renaissance over recent years propelled by new insight regarding their intimate coupling to synaptic transmission and a number of neurological disorders. It has long been surmised that the involvement of astrocytes in physiological and pathophysiological processes depends heavily on their key roles in K^+ and water homeostasis. Precise regulation of $[K^+]_o$ and volume is a prerequisite for normal brain function and a key element in the maintenance of an appropriate *milieu interne.*

A major step towards a better understanding of the mechanisms of K^+ and water homeostasis came with the identification of two families of proteins – the inwardly rectifying K^+ (Kir) channels and aquaporin (AQP) water channels. These proteins had properties that made them uniquely qualified as putative mediators of K^+ and water handling in the CNS. The present work was initiated to substantiate the idea that Kir and AQP proteins serve as molecular correlates of brain K^+ and volume homeostasis. Emphasis was placed on the predominant Kir and AQP isoforms in brain: Kir4.1 and AQP4.

Genetic manipulation was considered essential for realizing the ambitious goals of the present work. To differentiate between astrocytic Kir4.1 and AQP4 and other pools of these proteins it was deemed necessary to have access to glial-conditional knockouts of the proteins in question. A glial-selective knockout of Kir4.1 was made available while a glial-selective knockout of *Aqp4* had to be made *de novo* in our own laboratory. Used in conjunction with other knockouts, engineered in house or elsewhere, the glial-selective knockouts enabled us identify specific functional roles of Kir4.1 and AQP4 in the rodent CNS.

In paper I we provide strong evidence that astrocytic Kir4.1 is critically involved in removing K^+ from active synapses by way of a process termed spatial buffering. By definition, removal of K^+ by spatial buffering is not associated with any water movement. We could show that this criterion was satisfied by demonstrating that Kir4.1 deletion failed to affect extracellular volume dynamics. Mutations in the gene encoding Kir4.1 are known to be associated with epilepsy. Thus, our paper reinforces the link between dysfunctional K^+ handling and neuronal hyperexcitability.

A question that has intrigued neuroscientists for years is what mechanisms are responsible for regulating extracellular space volume in brain. Electron micrographs and functional analyses tell us that baseline volume is rather constant across time and brain region. While control of baseline volume is essential, it is also of interest to identify those mechanisms that are responsible for the rapid changes in extracellular space volume that occur in the wake of high frequency synaptic stimulation. Our hypothesis was that AQP4 is involved in both types of volume regulation.

In paper II we provided evidence that astrocytic AQP4 serves to shunt water into the extracellular space so as to dampen the rapid extracellular volume decrease that follows on the heels of synaptic activation. A priori, we were open as to the direction of AQP4 mediated water flow. Given the bidirectional water flux through AQP4, AQP4 could just as well be held responsible for mediating rather than counteracting the activity-dependent volume decrease. When the experimental data were indicative of a water flux that served to conserve extracellular volume, this is very much in line with the very definition of a homeostatic role.

To demonstrate a role of AQP4 in regulating baseline extracellular volume is a more challenging task. In paper IV we decided to take advantage of the fact that baseline extracellular volume is much decreased in the first postnatal weeks. If AQP4 is involved in controlling extracellular volume, a deletion of this protein would delay postnatal water resorption from the extracellular space. Our findings in a glial- conditional *Aqp4*$^{-/-}$ mouse line were consistent with this idea. Further, *Aqp4*$^{-/-}$ mouse lines, both glial-conditional and global, show increased brain water content consistent with an increased extracellular space volume. Taken together, our data suggest that AQP4 sets baseline extracellular volume and helps preserve extracellular volume in the face of high frequency synaptic stimulation.

Another key question is whether AQP4 is involved in the regulation of water exchange across the blood brain interface. To address this issue we had to resort to an experimental situation – hypo-osmotic stress - that affords a large flux of water across this interface. Even if this must be considered a pathophysiological condition, it should be informative as to the mechanisms that govern exchange of water in a physiological context. The glia-conditional *Aqp4* knockout was indispensable, as earlier studies failed to resolve whether AQP4 is also expressed

in endothelial cells. In the glial-conditional *Aqp4*$^{-/-}$ mice, no signal for AQP4 remained in immunoblots, nor was there any residual AQP4 immunogold signal at the blood-brain interface. Thus we could conclude that endothelial signals for AQP4 – observed in previous studies – were likely to represent contamination from the astrocytic pool. Brains of glial- conditional *Aqp4*$^{-/-}$ animals showed reduced uptake of water after hypo-osmotic stress, indicating that the astrocytic endfoot pool of AQP4 regulates water exchange at the brain-interface. This finding changes in a fundamental way our view of the blood-brain barrier as it confers a barrier function on the perivascular astrocytic endfeet.

Global *Aqp4* knockout altered the organization of the perivascular protein scaffold (paper III), but this perturbation did not affect endothelial permeability and expression of tight junction proteins. These data were critical for an appropriate understanding of the functional role of AQP4 in the CNS and for a correct interpretation of the physiological and pathophysiological effects observed after *Aqp4* deletion.

In conclusion, our studies have provided new insight in the roles of astrocytes in the CNS and demonstrated that the astrocytic pools of Kir4.1 and AQP4 serve key roles in brain K^+ and water homeostasis.

THE CANDIDATE'S EXPERIMENTAL CONTRIBUTION

Paper 1: Evidence that compromised K^+ spatial buffering contributes to the epileptogenic effect of mutations in the human Kir4.1 gene (KCNJ10)

- Immunofluorescence experiments
- Confocal microscopy
- Recordings of extracellular K^+ and TMA^+ in acute hippocampal slices
- Analysis of the K^+ and TMA^+ data
- Provided text for the manuscript

Paper II: Aquaporin-4 regulates extracellular space volume dynamics during high-frequency synaptic stimulation: a gene deletion study in mouse hippocampus

- Immunofluorescence experiments
- Confocal microscopy
- Recordings of extracellular TMA^+ in acute hippocampal slices
- Analysis of the TMA^+ data
- Contributed text to the Discussion of the manuscript

Paper III: Deletion of aquaporin-4 changes the perivascular glial protein scaffold without disrupting the endothelial barrier

- Immunofluorescence experiments
- Confocal microscopy

Paper IV: Glial-conditional deletion of aquaporin-4 (*Aqp4*) reduces blood-brain water uptake and confers barrier function on perivascular astrocyte endfeet

- Immunofluorescence experiments
- Confocal microscopy
- Measurements of whole brain basal water content and data analysis
- Contributed text to the manuscript

REFERENCES

Abbott, N. J., A. A. Patabendige, et al. (2010). "Structure and function of the blood-brain barrier." Neurobiol Dis **37**(1): 13-25.

Abbott, N. J., L. Ronnback, et al. (2006). "Astrocyte-endothelial interactions at the blood-brain barrier." Nat Rev Neurosci **7**(1): 41-53.

Adams, M. E., H. A. Mueller, et al. (2001). "In vivo requirement of the alpha-syntrophin PDZ domain for the sarcolemmal localization of nNOS and aquaporin-4." J Cell Biol **155**(1): 113-122.

Agre, P. (2004). "Aquaporin water channels (Nobel Lecture)." Angew Chem Int Ed Engl **43**(33): 4278-4290.

Amiry-Moghaddam, M., H. Lindland, et al. (2005). "Brain mitochondria contain aquaporin water channels: evidence for the expression of a short AQP9 isoform in the inner mitochondrial membrane." FASEB J **19**(11): 1459-1467.

Amiry-Moghaddam, M., T. Otsuka, et al. (2003). "An alpha-syntrophin-dependent pool of AQP4 in astroglial end-feet confers bidirectional water flow between blood and brain." Proc Natl Acad Sci U S A **100**(4): 2106-2111.

Amiry-Moghaddam, M. and O. P. Ottersen (2003). "The molecular basis of water transport in the brain." Nat Rev Neurosci **4**(12): 991-1001.

Amiry-Moghaddam, M., A. Williamson, et al. (2003). "Delayed K+ clearance associated with aquaporin-4 mislocalization: phenotypic defects in brains of alpha-syntrophin-null mice." Proc Natl Acad Sci U S A **100**(23): 13615-13620.

Badaut, J. (2010). "Aquaglyceroporin 9 in brain pathologies." Neuroscience **168**(4): 1047-1057.

Badaut, J., F. Lasbennes, et al. (2002). "Aquaporins in brain: distribution, physiology, and pathophysiology." J Cereb Blood Flow Metab **22**(4): 367-378.

Bass, N. H., H. H. Hess, et al. (1971). "Quantitative cytoarchitectonic distribution of neurons, glia, and DNa in rat cerebral cortex." J Comp Neurol **143**(4): 481-490.

Bergersen, L., E. Johannsson, et al. (1999). "Cellular and subcellular expression of monocarboxylate transporters in the pigment epithelium and retina of the rat." Neuroscience **90**(1): 319-331.

Binder, D. K., X. Yao, et al. (2006). "Increased seizure duration and slowed potassium kinetics in mice lacking aquaporin-4 water channels." Glia **53**(6): 631-636.

Bockamp, E., R. Sprengel, et al. (2008). "Conditional transgenic mouse models: from the basics to genome-wide sets of knockouts and current studies of tissue regeneration." Regen Med **3**(2): 217-235.

Boron Walter, E. B. (2005). Physiology of cells and molecules. Medical Physiology. Philadelphia, Elsevier Inc**:** 1319.

Bushong, E. A., M. E. Martone, et al. (2002). "Protoplasmic astrocytes in CA1 stratum radiatum occupy separate anatomical domains." J Neurosci **22**(1): 183-192.

Cardoso, F. L., D. Brites, et al. (2010). "Looking at the blood-brain barrier: molecular anatomy and possible investigation approaches." Brain Res Rev **64**(2): 328-363.

Cogan, M. (1991). Normal Potassium Homeostasis. Fluids and Electrolytes -Physiology and Pathophysiology, Appleton and Lange**:** 125.

Connors, N. C., M. E. Adams, et al. (2004). "The potassium channel Kir4.1 associates with the dystrophin-glycoprotein complex via alpha-syntrophin in glia." J Biol Chem **279**(27): 28387-28392.

Danbolt, N. C., F. A. Chaudhry, et al. (1998). "Properties and localization of glutamate transporters." Prog Brain Res **116**: 23-43.

Elkjaer, M., Z. Vajda, et al. (2000). "Immunolocalization of AQP9 in liver, epididymis, testis, spleen, and brain." Biochem Biophys Res Commun **276**(3): 1118-1128.

Frigeri, A., M. A. Gropper, et al. (1995). "Immunolocalization of the mercurial-insensitive water channel and glycerol intrinsic protein in epithelial cell plasma membranes." Proc Natl Acad Sci U S A **92**(10): 4328-4331.

Frigeri, A., G. P. Nicchia, et al. (2001). "Aquaporin-4 deficiency in skeletal muscle and brain of dystrophic mdx mice." FASEB J **15**(1): 90-98.

Furman, C. S., D. A. Gorelick-Feldman, et al. (2003). "Aquaporin-4 square array assembly: opposing actions of M1 and M23 isoforms." Proc Natl Acad Sci U S A **100**(23): 13609-13614.

Garcia-Marin, V., P. Garcia-Lopez, et al. (2007). "Cajal's contributions to glia research." Trends Neurosci **30**(9): 479-487.

Gaveriaux-Ruff, C. and B. L. Kieffer (2007). "Conditional gene targeting in the mouse nervous system: Insights into brain function and diseases." Pharmacol Ther **113**(3): 619-634.

Gomes, D., A. Agasse, et al. (2009). "Aquaporins are multifunctional water and solute transporters highly divergent in living organisms." Biochim Biophys Acta **1788**(6): 1213-1228.

Haydon, P. G. and G. Carmignoto (2006). "Astrocyte control of synaptic transmission and neurovascular coupling." Physiol Rev **86**(3): 1009-1031.

Higashi, K., A. Fujita, et al. (2001). "An inwardly rectifying K(+) channel, Kir4.1, expressed in astrocytes surrounds synapses and blood vessels in brain." Am J Physiol Cell Physiol **281** (3): C922-931.

Ishibashi, K., S. Koike, et al. (2009). "The role of a group III AQP, AQP11 in intracellular organelle homeostasis." J Med Invest **56 Suppl**: 312-317.

Jung, J. S., R. V. Bhat, et al. (1994). "Molecular characterization of an aquaporin cDNA from brain: candidate osmoreceptor and regulator of water balance." Proc Natl Acad Sci U S A **91**(26): 13052-13056.

Karwoski, C. J., H. K. Lu, et al. (1989). "Spatial buffering of light-evoked potassium increases by retinal Muller (glial) cells." Science **244**(4904): 578-580.

Kimelberg, H. K. (2004). "Water homeostasis in the brain: basic concepts." Neuroscience **129**(4): 851-860.

Kimelberg, H. K. and M. Nedergaard (2010). "Functions of astrocytes and their potential as therapeutic targets." Neurotherapeutics **7**(4): 338-353.

King, L. S., D. Kozono, et al. (2004). "From structure to disease: the evolving tale of aquaporin biology." Nat Rev Mol Cell Biol **5**(9): 687-698.

Kofuji, P. and E. A. Newman (2004). "Potassium buffering in the central nervous system." Neuroscience **129**(4): 1045-1056.

Krawczyk, A. and J. Jaworska-Adamu (2010). "Synantocytes: the fifth type of glia? In comparison with astrocytes." Folia Histochem Cytobiol **48**(2): 173-177.

Lodish H, B. A., Zipursky SL, et al. (2000). Gene Replacement and transgenic Animals. Cell Biology. New York, W.H.Freeman and Company.

Lumeng, C. N., M. Hauser, et al. (1999). "Expression of the 71 kDa dystrophin isoform (Dp71) evaluated by gene targeting." Brain Res **830**(1): 174-178.

MacAulay, N., S. Hamann, et al. (2004). "Water transport in the brain: role of cotransporters." Neuroscience **129**(4): 1031-1044.

MacAulay, N. and T. Zeuthen (2010). "Water transport between CNS compartments: contributions of aquaporins and cotransporters." Neuroscience **168**(4): 941-956.

Manley, G. T., M. Fujimura, et al. (2000). "Aquaporin-4 deletion in mice reduces brain edema after acute water intoxication and ischemic stroke." Nat Med **6**(2): 159-163.

Moody, D. M. (2006). "The blood-brain barrier and blood-cerebral spinal fluid barrier." Semin Cardiothorac Vasc Anesth **10**(2): 128-131.

Morozov, A. (2008). "Conditional gene expression and targeting in neuroscience research." Curr Protoc Neurosci **Chapter 4**: Unit 4 31.

Muntoni, F., S. Torelli, et al. (2003). "Dystrophin and mutations: one gene, several proteins, multiple phenotypes." Lancet Neurol **2**(12): 731-740.

Nagelhus, E. A., Y. Horio, et al. (1999). "Immunogold evidence suggests that coupling of K+ siphoning and water transport in rat retinal Muller cells is mediated by a coenrichment of Kir4.1 and AQP4 in specific membrane domains." Glia **26**(1): 47-54.

Nagelhus, E. A., T. M. Mathiisen, et al. (2004). "Aquaporin-4 in the central nervous system: cellular and subcellular distribution and coexpression with KIR4.1." Neuroscience **129** (4): 905-913.

Nagelhus, E. A., M. L. Veruki, et al. (1998). "Aquaporin-4 water channel protein in the rat retina and optic nerve: polarized expression in Muller cells and fibrous astrocytes." J Neurosci **18**(7): 2506-2519.

Nagy, A. (2000). "Cre recombinase: the universal reagent for genome tailoring." Genesis **26**(2): 99-109.

Nedergaard, M., B. Ransom, et al. (2003). "New roles for astrocytes: redefining the functional architecture of the brain." Trends Neurosci **26**(10): 523-530.

Neely, J. D., M. Amiry-Moghaddam, et al. (2001). "Syntrophin-dependent expression and localization of Aquaporin-4 water channel protein." Proc Natl Acad Sci U S A **98**(24): 14108-14113.

Neely, J. D., B. M. Christensen, et al. (1999). "Heterotetrameric composition of aquaporin-4 water channels." Biochemistry **38**(34): 11156-11163.

Newman, E. A., D. A. Frambach, et al. (1984). "Control of extracellular potassium levels by retinal glial cell K+ siphoning." Science **225**(4667): 1174-1175.

Nicchia, G. P., A. Rossi, et al. (2010). "Higher order structure of aquaporin-4." Neuroscience **168** (4): 903-914.

Nicchia, G. P., A. Rossi, et al. (2008). "Dystrophin-dependent and -independent AQP4 pools are expressed in the mouse brain." Glia **56**(8): 869-876.

Nico, B., G. Paola Nicchia, et al. (2004). "Altered blood-brain barrier development in dystrophic MDX mice." Neuroscience **125**(4): 921-935.

Nielsen, S., E. A. Nagelhus, et al. (1997). "Specialized membrane domains for water transport in glial cells: high-resolution immunogold cytochemistry of aquaporin-4 in rat brain." J Neurosci **17**(1): 171-180.

Nielsen, S., B. L. Smith, et al. (1993). "Distribution of the aquaporin CHIP in secretory and resorptive epithelia and capillary endothelia." Proc Natl Acad Sci U S A **90**(15): 7275-7279.

Oberheim, N. A., X. Wang, et al. (2006). "Astrocytic complexity distinguishes the human brain." Trends Neurosci **29**(10): 547-553.

Orkand, R. K. (1986). "Glial-interstitial fluid exchange." Ann N Y Acad Sci **481**: 269-272.

Oshio, K., H. Watanabe, et al. (2005). "Reduced cerebrospinal fluid production and intracranial pressure in mice lacking choroid plexus water channel Aquaporin-1." FASEB J **19**(1): 76-78.

Papadopoulos, M. C., G. T. Manley, et al. (2004). "Aquaporin-4 facilitates reabsorption of excess fluid in vasogenic brain edema." FASEB J **18**(11): 1291-1293.

Papadopoulos, M. C. and A. S. Verkman (2007). "Aquaporin-4 and brain edema." Pediatr Nephrol **22**(6): 778-784.

Pekny, M., U. Wilhelmsson, et al. (2007). "The role of astrocytes and complement system in neural plasticity." Int Rev Neurobiol **82**: 95-111.

Preston, G. M., T. P. Carroll, et al. (1992). "Appearance of water channels in Xenopus oocytes expressing red cell CHIP28 protein." Science **256**(5055): 385-387.

Puwarawuttipanit, W., A. D. Bragg, et al. (2006). "Differential effect of alpha-syntrophin knockout on aquaporin-4 and Kir4.1 expression in retinal macroglial cells in mice." Neuroscience **137**(1): 165-175.

Ransom, B., T. Behar, et al. (2003). "New roles for astrocytes (stars at last)." Trends Neurosci **26** (10): 520-522.

Rash, J. E., T. Yasumura, et al. (1998). "Direct immunogold labeling of aquaporin-4 in square arrays of astrocyte and ependymocyte plasma membranes in rat brain and spinal cord." Proc Natl Acad Sci U S A **95**(20): 11981-11986.

Reese, T. S. and M. J. Karnovsky (1967). "Fine structural localization of a blood-brain barrier to exogenous peroxidase." J Cell Biol **34**(1): 207-217.

Ruiz-Ederra, J., H. Zhang, et al. (2007). "Evidence against functional interaction between aquaporin-4 water channels and Kir4.1 potassium channels in retinal Muller cells." J Biol Chem **282**(30): 21866-21872.

Saunders, N. R., C. J. Ek, et al. (2008). "Barriers in the brain: a renaissance?" Trends Neurosci **31**(6): 279-286.

Simard, M., G. Arcuino, et al. (2003). "Signaling at the gliovascular interface." J Neurosci **23** (27): 9254-9262.

Simard, M. and M. Nedergaard (2004). "The neurobiology of glia in the context of water and ion homeostasis." Neuroscience **129**(4): 877-896.

Soe, R., N. Macaulay, et al. (2009). "Modulation of Kir4.1 and Kir4.1-Kir5.1 channels by small changes in cell volume." Neurosci Lett **457**(2): 80-84.

Sykova, E. and C. Nicholson (2008). "Diffusion in brain extracellular space." Physiol Rev **88**(4): 1277-1340.

Vajda, Z., M. Pedersen, et al. (2002). "Delayed onset of brain edema and mislocalization of aquaporin-4 in dystrophin-null transgenic mice." Proc Natl Acad Sci U S A **99**(20): 13131-13136.

van der Neut, R. (1997). "Targeted gene disruption: applications in neurobiology." J Neurosci Methods **71**(1): 19-27.

Verbavatz, J. M., T. Ma, et al. (1997). "Absence of orthogonal arrays in kidney, brain and muscle from transgenic knockout mice lacking water channel aquaporin-4." J Cell Sci **110 (Pt 22)**: 2855-2860.

Verkman, A. S. (2009). "Aquaporins: translating bench research to human disease." J Exp Biol **212**(Pt 11): 1707-1715.

Wen, H., E. A. Nagelhus, et al. (1999). "Ontogeny of water transport in rat brain: postnatal expression of the aquaporin-4 water channel." Eur J Neurosci **11**(3): 935-945.

Wilhelmsson, U., E. A. Bushong, et al. (2006). "Redefining the concept of reactive astrocytes as cells that remain within their unique domains upon reaction to injury." Proc Natl Acad Sci U S A **103**(46): 17513-17518.

Wolburg, H. (1995). "Orthogonal arrays of intramembranous particles: a review with special reference to astrocytes." J Hirnforsch **36**(2): 239-258.

Wolburg, H., S. Noell, et al. (2009). "Agrin, aquaporin-4, and astrocyte polarity as an important feature of the blood-brain barrier." Neuroscientist **15**(2): 180-193.

Wynsberghe Donna, N. C., Carola Robert (1995). Introduction to Anatomy and Physiology. Human Anatomy and Physiology, McGraw-Hill.

Yao, X., S. Hrabetova, et al. (2008). "Aquaporin-4-deficient mice have increased extracellular space without tortuosity change." J Neurosci **28**(21): 5460-5464.

Zelenina, M. (2010). "Regulation of brain aquaporins." Neurochem Int **57**(4): 468-488.

I

II

Aquaporin-4 regulates extracellular space volume dynamics during high-frequency synaptic stimulation: a gene deletion study in mouse hippocampus

Abbreviated title: AQP4 regulates extracellular space volume dynamics

Nadia Nabil Haj-Yasein,[1,2*] Vidar Jensen,[1,2*] Ivar Østby,[3] Stig Omholt,[4] Juha Voipio,[5] Kai Kaila,[5] Ole Petter Ottersen,[2] Øivind Hvalby[2], and Erlend A. Nagelhus[1,2,6,7]

[1]Centre for Molecular Medicine Norway, Nordic EMBL Partnership, University of Oslo, 0318 Oslo, Norway.

[2]Centre for Molecular Biology and Neuroscience, Letten Centre, Institute of Basic Medical Sciences, University of Oslo, 0317 Oslo, Norway.

[3]Department of Mathematical Sciences and Technology, Norwegian University of Life Sciences, 1430 Ås, Norway.

[4]Centre for Integrative Genetics (CIGENE), Norwegian University of Life Sciences, 1432 Ås, Norway.

[5]Department of Biosciences and Neuroscience Center, University of Helsinki, FI-00014 Helsinki, Finland.

[6]Oslo University Hospital, Department of Neurology, 0027 Oslo, Norway.

[7]Center for Translational Neuromedicine, Division of Glial Disease and Therapeutics, Department of Neurosurgery, University of Rochester Medical Center, Rochester, New York 14642.

*These authors contributed equally

Corresponding author: Dr. Erlend A. Nagelhus, Centre for Molecular Medicine Norway, Nordic EMBL Partnership, University of Oslo, P.O. Box 1137 Blindern, N-0318 Oslo, Norway. Phone: +4791736316. Fax: +4722851278. E-mail: e.a.nagelhus@ncmm.uio.no

Number of pages: 22

Number of figures: 4

Number of tables: 0

Number of words for abstract: 162

Number of words for Introduction: 382

Number of words for Discussion: 727

Total number of words: 4592

Conflicts of interest: None

ACKNOWLEDGEMENTS

We thank Cecilie E. Bugge, Centre for Molecular Medicine Norway, Gaute Nesse, Oslo University Hospital, Carina Knutsen and Gunnar F. Lothe, Institute of Basic Medical Sciences, for technical assistance. This work was supported by the Research Council of Norway and Letten Foundation.

ABSTRACT

Little is known about the physiological roles of aquaporin-4 (AQP4) in the central nervous system. AQP4 water channels are concentrated in endfeet membranes of astrocytes but also localize to the fine astrocytic processes that abut on central synapses. Based on its pattern of expression we predicted that AQP4 could be involved in controlling water fluxes and changes in extracellular space (ECS) volume that are associated with activation of excitatory pathways. Here we show that deletion of *Aqp4* accentuated the shrinkage of the ECS that occured in the mouse hippocampal CA1 region during activation of Schaffer collateral/commissural fibres. This effect was found in the stratum radiatum (where perisynaptic astrocytic processes abound) but not in the pyramidal cell layer (where astrocytic processes constitute but a minor volume fraction). For both genotypes the ECS shrinkage was most pronounced in the pyramidal cell layer. Our data attribute a physiological role to AQP4 and indicate that this water channel regulates extracellular volume dynamics in the mammalian brain.

INTRODUCTION

What are the factors that regulate the extracellular space volume in brain? Despite its importance, this question has not received much attention. One aspect is the baseline volume; another fundamental aspect is the extracellular volume dynamics coupled to synaptic activity. More than three decades ago it was shown that evoked synaptic activity is followed by a rapid shrinkage of the ECS (Dietzel et al., 1980). The shrinkage is substantial, amounting to 4-30%, depending on the mode of stimulation, type of preparation, and area under investigation (Dietzel et al., 1980; Holthoff and Witte, 1996; Sykova et al., 2003; Viitanen et al., 2010).

Extracellular volume changes have a significant impact on the concentration of extracellular solutes and vice versa. Synaptic stimulation causes release of a number of solutes that are removed through cotransport with water (MacAulay and Zeuthen, 2010). Essential among these is K^+, which is cleared by a multitude of mechanisms including chloride coupled uptake into glia (Kofuji and Newman, 2004; Ostby et al., 2009). Likewise, glial uptake of bicarbonate and glutamate is associated with water transport and may contribute to the observed shrinkage of the ECS (Nagelhus et al., 2004). Extracellular volume changes are also implicated in a number of pathophysiological conditions such as spreading depression and are known to precede seizure activity (Olsson et al., 2006).

With the discovery of water channels in brain, the question arose whether these are involved in ECS volume dynamics. AQP4 - the predominant brain water channel – is enriched in those astrocytic plasma membrane domains that face vessels and pia but is also expressed in the delicate astrocyte processes that abut on excitatory synapses (Nielsen et al., 1997). AQP4 water channels in the latter processes are unlikely to be passive bystanders to the local volume dynamics. If involved, the perisynaptic AQP4 pool could either curb or accentuate the activity-dependent shrinkage of the ECS.

Here we show that the activity-dependent ECS shrinkage is more pronounced in animals lacking AQP4 than in wild-type animals. Our data indicate that perisynaptic AQP4 serves to blunt the activity-dependent volume decrease. This would occur if activity-coupled cotransport of water into perisynaptic glia normally is associated with a passive, AQP4-mediated water flux in the opposite direction. Thus, our data indicate that AQP4 serves an important homeostatic function that may represent the elusive physiological role of this aquaporin.

MATERIALS AND METHODS

Animals

Constitutive *Aqp4*$^{-/-}$ mice were generated as described previously (Thrane et al., 2011). For characterization of synaptic transmission and plasticity we used *Aqp4*$^{-/-}$ and wild-type (WT) siblings obtained from heterozygous breeding pairs. After backcrossing to C57BL/6J mice for five generations (Jackson Laboratories, Maine, USA), we used *Aqp4*$^{-/-}$ mice from mutant breeders and C57BL/6J mice as WT controls. Studies were conducted with mice aged 8-18 weeks, weighing 20-30g. All experiments were approved by the institution's Animal Care and Use Committee.

Immunocytochemistry

The animals were deeply anesthetized with a mixture of chloral hydrate, magnesium sulfate and pentobarbital (142, 70 and 32 mg/kg body weight i.p., respectively) before transcardiac perfusion with 0.1 M phosphate buffer (PB; pH 7.4) with 2% dextran for 15-20 s, followed by the fixative for 15-20 min (flow rate ~8 ml/min). For light microscopic (LM) cytochemistry we used 4% formaldehyde in PB and for electron microscopic (EM) cytochemistry we used 4% formaldehyde in PB containing 0.2% picric acid at pH 6.0, followed by a similar fixative at pH 10.0 (Nagelhus et al., 1998). For LM experiments the brain was cryoprotected in sucrose (10%, 20% and 30% in PB), and sections were cut at 15 μm on a cryostat.

Immunofluorescence

LM immunocytochemistry was carried out using an indirect fluorescence method (Veruki and Wassle, 1996). The concentrations of antibodies were: rabbit anti-AQP4 (Millipore), 2 μg/ml; chicken anti-GFAP (Nordic BioSite Covance), 40 μg/ml; mouse anti-Neuronal Nuclei (NeuN; Chemicon) 10 μg/ml. Cortical sections were viewed and photographed with a Zeiss LSM 5 PASCAL microscope equipped with epifluorescence optics, using an m2 filter (BP 546/14, RKP 580, and LP 580) and 40X/1.3 Oil Plan-Neofluar objective.

Electron microscopic immunocytochemistry

Small blocks of fixed cortex from WT and *Aqp4*$^{-/-}$ mice were subjected to freeze substitution as described previously (Nielsen et al., 1997). Ultrathin sections were cut with a Reichert ultramicrotome, mounted on nickel grids, and processed for immunogold cytochemistry. The sections were incubated sequentially in the following solutions (at room temperature): (1) 50

mM glycine in Tris buffer (5 mM) containing 0.01% Triton X-100 and 50mM NaCl (TBST; 10 min); (2) 2% human serum albumin (HSA) in TBST (10 min); (3) primary antibody (anti-AQP4 from Millipore, 20 μg/ml) diluted in the solution used in the preceding step (overnight); (4) same solution as in step 2 (10 min x 2); (5) gold-conjugated IgG (GAR10 nm; Abcam), diluted 1:20 in TBST containing 2% HSA and polyethylene glycol (0.5 mg/ml, 1 h). Finally, the sections were counterstained and examined in a Fei Tecnai 12 transmission electron microscope.

Electrophysiology

Synaptic transmission and synaptic plasticity. Adult (>P60) mutant mice and their control littermates were anaesthetized with Suprane (Baxter) and decapitated. Brains were removed and transverse slices (400 μm) were cut from each hippocampus with a vibroslicer in cold artificial cerebrospinal fluid (ACSF) containing (in mM): 124 NaCl, 2 KCl, 1.25 KH_2PO_4, 2 $MgSO_4$, 2 $CaCl_2$, 26 $NaHCO_3$ and 12 glucose, bubbled with 95% O_2 / 5% CO_2 (pH 7.3 at the experimental temperature). Slices were placed in a humidified interface chamber at 28-32^{o}C and perfused with ACSF. Orthodromic synaptic stimuli (<300 μA, 0.1 Hz) were delivered through a monopolar tungsten electrode placed in stratum radiatum. The presynaptic volley and the field excitatory postsynaptic potential (fEPSP) were recorded by a glass microelectrode (filled with ACSF) placed in stratum radiatum, while another microelectrode, placed in the pyramidal cell body layer monitored the population spike. Following a period with stable responses, we stimulated the afferent fibers with increasing strength (increasing the stimulus duration in steps of 10 μs from 0 to 90 μs, five consecutive stimulations at each

step). A similar approach was used to elicit paired-pulse responses (50 ms interstimulus interval, the two stimuli being equal in strength).

To assess synaptic transmission, we measured the amplitude of the presynaptic volley and fEPSP at different stimulation strengths. The population spike amplitude was measured between the maximal population spike peak and a line joining the maximum prespike and postspike positivities. In order to pool data from the paired-pulse experiments we selected responses to a stimulation strength just below the threshold for eliciting a population spike on the second fEPSP. To compare the frequency facilitation and the delayed response enhancement (DRE) in the two genotypes, we analyzed synaptic strength during a 20 Hz stimulation train (1 min). The maximal slope of the rising phase of the fEPSP (V/s) was normalized to the mean value recorded just prior to the 20 Hz train. To analyze long-term potentiation of synaptic transmission (LTP), orthodromic synaptic stimulation in CA1 was delivered alternately through two tungsten electrodes (0.2 Hz) activating synapses in apical (stratum radiatum) and basal dendrites (stratum oriens), respectively. The fEPSPs were monitored by glass microelectrodes filled with ACSF placed in the corresponding synaptic layers. The radiatum pathway was tetanized (100 Hz, 1 s), whereas the oriens pathway served as control. The tetanic stimulation strength was set in response to a single shock at an intensity just above the threshold for generating a population spike. Synaptic efficacy was assessed by measuring the slope of the fEPSP in the middle third of its rising phase. Six consecutive responses (1 min) were averaged and normalized to the mean value recorded 4-7 min prior to tetanic stimulation.

Extracellular volume measurements. Ion-selective microelectrodes were made from non-filamented micropipettes that were silanized and filled with 150 mM tetramethylammonium (TMA^+) chloride (Sigma Life Science). The electrode tip was filled with the liquid ion exchanger (IE190; World Precision Instruments Inc.) by gentle suction, as

described previously (Voipio et al., 1994). The electrodes were calibrated in ACSF containing different concentrations of TMA^+ (in mM: 1.5, 2.0, and 3.0 mM). The log-linear fit was used to calculate the [TMA^+] in the ECS from each experiment.

Orthodromic synaptic stimuli (<300 μA, 50 μs, 0.1 Hz) were delivered through a tungsten electrode placed in stratum radiatum in the CA1 region. The responses were monitored by the reference glass microelectrode (filled with ACSF) placed close to the ion sensitive microelectrode in stratum radiatum at a distance of 400 μm from the stimulation electrode (Fig. 1*A*). Signal from the reference microelectrode was subtracted from that of the ion sensitive microelectrode (custombuilt electrometer/differential amplifier, 2 Hz LPF) in order to get a signal that reflects only the [TMA^+] in the ECS. We used a stimulation strength which was just above eliciting a detectable population spike in the radiatum recording electrode. Following a period with stable responses, we stimulated the Schaffer collateral/commissural fibres at 20 Hz frequency with a 60 s stimulation train. We also compared the responses in the synaptic and soma layers in the same slice in some experiments by moving the recording electrodes from stratum radiatum to stratum pyramidale or vice versa.

In the experiments 1.5 mM TMA^+ was added to the ACSF. TMA^+ is mainly localized to the ECS (Nicholson and Phillips, 1981). Since the ion exchanger IE190 used here is far more sensitive to TMA^+ than to K^+, changes in $[TMA^+]_o$ will reflect changes in ECS volume (Sykova and Nicholson, 2008). Control experiments indicated that the equilibration of TMA^+ between the bath and the slice was slow enough to be ignored in the analysis of the present ECS volume data (wash-in of TMA^+ (min); WT, n = 7, 19.1 ± 2.6; *Aqp4*$^{-/-}$, n = 5, 18.0 ± 1.3). Relative alteration in ECS volume was calculated as follows:

% change of ECS = ((baseline $[TMA^+]_o$)/($[TMA^+]_o$) - 1) x 100

Data are presented as mean ± SEM. For comparison between genotypes we used a linear mixed model statistical analysis (SAS 9.2) if not otherwise stated.

RESULTS

Immunofluorescence revealed AQP4-labeling of GFAP-immunopositive cells in stratum radiatum and pyramidale of wild-type mice, indicating expression of AQP4 in astrocytes (Fig. 1*A-D,F*). The labeling pattern in acute slices did not differ from that in perfusion-fixed tissue (compare *A* and *D* in Fig. 1). Absence of AQP4 labeling in *Aqp4* knockout animals confirmed the genotype and the selectivity of antibodies (Fig. 1*E*). High resolution immunogold cytochemistry confirmed AQP4 labeling of astrocytic membranes, both around synapses in stratum radiatum and interspersed between neuronal somata in stratum pyramidale (Fig. 2*A,B*). The density of gold particles over these membrane domains was lower than that of astrocytic membranes abutting on microvessels (Fig. 2*C*). The ultrastructure of WT (Fig. 2*A-C*) and *Aqp4*$^{-/-}$ mice (Fig. 2*D-F*) was indistinguishable. Absence of immunogold particles over astrocytic membranes in the mutant mice attests to the selectivity of antibodies (Fig. 2*D-F*).

In slices obtained from WT animals, activation of Schaffer collateral/commissural fibers led to a rapid and pronounced decrease in ECS volume in stratum radiatum, as judged by use of the impermeant cation TMA^+ (Fig. 3*A-B*). In *Aqp4*$^{-/-}$ mice the shrinkage of the ECS was accentuated by ~30% compared with WT (Fig. 3*B,C*).

The data from stratum radiatum were compared with data from stratum pyramidale. In both WT and *Aqp4*$^{-/-}$ mice stratum pyramidale showed a more pronounced ECS shrinkage

during synaptic stimulation than did stratum radiatum (Fig. 3*D*; WT, volume change in radiatum: -5.06% ± 0.66; WT, pyramidale: -8.96% ± 1.08; *Aqp4*$^{-/-}$, radiatum: -7.46% ± 1.15; *Aqp4*$^{-/-}$, pyramidale: -10.23% ± 1.21). In contrast to stratum radiatum, the ECS shrinkage in stratum pyramidale was not accentuated by *Aqp4* deletion ($p>0.05$; Fig. 3*D*).

To assess whether the changes in ECS volume dynamics could be secondary to changes in excitatory synaptic transmission and synaptic excitability, we recorded field-potential responses simultaneously in the apical dendritic and soma layers in the CA1 region of hippocampal slices. The stimulation strengths necessary to elicit fibre volleys with defined amplitudes (0.5, 1.0 and 1.5 mV) were not significantly different in the two genotypes (WT: 5.4 ± 0.4 nC; 10.0 ± 0.8 nC; 14.5 ± 1.4 nC; *Aqp4*$^{-/-}$: 4.8 ± 0.4 nC; 8.5 ± 0.8 nC; 10.7 ± 1.1 nC; n ranged from 20 to 32) (Fig. 4*A*). The magnitudes of the evoked fEPSPs elicited by fibre volleys of the defined amplitudes were also similar (WT: 2.0 ± 0.1 mV; 3.1 ± 0.1 mV; 3.6 ± 0.2 mV; *Aqp4*$^{-/-}$: 1.7 ± 0.2 mV; 2.8 ± 0.2 mV; 3.6 ± 0.2 mV; n ranged from 20 to 32) (Fig. 4*B,E*), indicating a similar efficacy of the excitatory synaptic transmission. Furthermore, we observed no differences in synaptic excitability when the threshold for generation of a population spike (WT mice: 2.3 ± 0.1 mV, n = 32; *Aqp4*$^{-/-}$: 2.3 ± 0.1 mV, n = 32) or a population spike of 2 mV amplitude (WT mice: 3.3 ± 0.2 mV, n = 32; *Aqp4*$^{-/-}$: 3.6 ± 0.2 mV, n = 30) were measured as a function of fEPSP amplitude (Fig. 4*C,E*). A comparison of paired-pulse facilitation at 50 ms stimulation interval failed to unmask a significant difference ($p = 0.12$) between WT (1.42 ± 0.02, n = 32) and *Aqp4*$^{-/-}$ (1.50 ± 0.02, n = 32) mice (Fig. 4*D,E*).

Other forms of short-term plasticity, like frequency facilitation and the delayed response enhancement (DRE) (Jensen et al., 2007), did not differ between the two genotypes and the fEPSPs followed a similar pattern during the subsequent period of low frequency synaptic activation (Fig. 4*F*).

In agreement with Skucas et al. (2010) a single tetanic stimulation (100 Hz, 1 s) of the afferent fibers in stratum radiatum produced a lasting, homosynaptic LTP of the same magnitude in both genotypes ($p = 0.83$; Fig 4*G*). The average fEPSP slope 40-45 min after tetanization was 1.30 ± 0.08 (n = 20) of the pretetanic control value in WT mice and 1.32 ± 0.05 (n = 18) in *Aqp4*$^{-/-}$ mice (Fig.4*G*).

DISCUSSION

The main finding in the present study is that deletion of *Aqp4* accentuates ECS volume changes associated with activation of excitatory synaptic pathways in the hippocampus. This would occur if, upon synaptic activation, AQP4 normally mediates a rapid water flux from perisynaptic astrocytic processes to the ECS so as to reduce activity-dependent ECS shrinkage. Such an explanation is in line with high resolution immunogold data that have revealed a distinct pool of AQP4 in the delicate astrocytic processes that ensheath central synapses (Nielsen et al., 1997). Thus, the present findings attribute a physiological role for perisynaptic AQP4.

The observed difference between WT and *Aqp4*$^{-/-}$ mice might be influenced by compensatory developmental changes in the mutants leading to altered synaptic transmission and excitability. A thorough electrophysiological analysis was required to rule out this experimental confound. This analysis showed that the lack of AQP4 did not affect key parameters of synaptic function and synaptic plasticity. In agreement, Skucas et al. (2011) recently reported that deletion of *Aqp4* did not impair basal synaptic transmission or short

term synaptic plasticity. However, the latter study indicated that *Aqp4* deletion interferes with a form of LTP induced by theta burst stimulation.

Activity-dependent shrinkage of the ECS is a robust phenomenon that was discovered more than three decades ago (Dietzel et al., 1980). Yet, detailed mechanistic insight into this phenomenon is still lacking. A local reduction in ECS volume must necessarily reflect uptake of water into adjacent cells – neurons, glia, or both. In agreement, swelling of glia and/or neurons is a hallmark of cortical spreading depression and glutamate receptor activation (Van and Khattab, 1967; Takano et al., 2007; Uckermann et al., 2004).

What drives net water uptake in post- or perisynaptic cells? Excitatory synaptic transmission is associated with release of K^+ and glutamate which are effectively removed from the ECS, primarily by uptake into glia. It is well documented that K^+ and glutamate uptake is coupled to water transport (MacAulay and Zeuthen, 2010). Similarly, activation of electrogenic bicarbonate transport subsequent to glial depolarization is a probable driver of water uptake (Nagelhus et al., 2004). In the case of neurons, water accumulation occurs secondary to Na^+ influx through activated AMPA receptors (Uckermann et al., 2004). Through these and other mechanisms, water uptake is coupled inextricably with synaptic transmission.

Our data indicate that activity-dependent water uptake is partly offset by an AQP4-mediated water flux operating in the opposite direction. Transport through AQP4 occurs along the concentration gradient of water. Thus we must hypothesize that synaptic activation causes a reduction in water concentration in the perisynaptic ECS and that this reduction is what drives passive water flux through AQP4. The reduction in water concentration may come about through solute release from activated neurons, through export of osmolytes from glia, through anisosmotic water cotransport into perisynaptic glia or neurons, or by a combination

of the above. In our recent modelling paper (Ostby et al., 2009) we predicted that a deletion of *Aqp4* would accentuate activity-dependent ECS shrinkage, but only if NKCC1 – the predominant Na-K-Cl cotransporter in brain - is allowed to transport water. NKCCl is assumed to play an important role in removing excess K^+ from the ECS around activated synapses (Kofuji and Newman, 2004) and inhibition of NKCC1 reduces activity-dependent ECS shrinkage (Holthoff and Witte, 1996). Thus, AQP4 may serve to partly counteract water redistribution caused by activation of synaptic homeostatic mechanisms and by NKCC1 activation in particular.

Our conclusion is that AQP4 normally serves to blunt the shrinkage of ECS by allowing water efflux from astrocytic processes. To corroborate our conclusion, we investigated activity-dependent volume changes in stratum pyramidale where neurons (that lack AQP4) predominate. Constituting but a tiny volume fraction, astrocytic processes would not be expected to impact extracellular volume in stratum pyramidale. In accordance, we found that *Aqp4* deletion failed to affect ECS volume dynamics in stratum pyramidale and that the magnitude of ECS shrinkage was higher in stratum pyramidale than in stratum radiatum. It is likely that the ECS shrinkage in the former layer primarily reflects expansion of the neuronal compartment.

The physiological role of AQP4 has proved difficult to identify and previous gene deletion studies have revealed but minor physiological changes mainly in sensory systems (Verkman et al., 2006). The present data indicate that AQP4 is involved in the regulation of ECS volume dynamics associated with excitatory synaptic transmission in the brain.

References

Dietzel I, Heinemann U, Hofmeier G, Lux HD (1980) Transient changes in the size of the extracellular space in the sensorimotor cortex of cats in relation to stimulus-induced changes in potassium concentration. Exp Brain Res 40:432-439.

Holthoff K, Witte OW (1996) Intrinsic optical signals in rat neocortical slices measured with near-infrared dark-field microscopy reveal changes in extracellular space. J Neurosci 16:2740-2749.

Jensen V, Walaas SI, Hilfiker S, Ruiz A, Hvalby O (2007) A delayed response enhancement during hippocampal presynaptic plasticity in mice. J Physiol 583:129-143.

Kofuji P, Newman EA (2004) Potassium buffering in the central nervous system. Neuroscience 129:1045-1056.

MacAulay N, Zeuthen T (2010) Water transport between CNS compartments: contributions of aquaporins and cotransporters. Neuroscience 168:941-956.

Nagelhus EA, Mathiisen TM, Ottersen OP (2004) Aquaporin-4 in the central nervous system: Cellular and subcellular distribution and coexpression with Kir4.1
1. Neuroscience 129:905-913.

Nagelhus EA, Veruki ML, Torp R, Haug FM, Laake JH, Nielsen S, Agre P, Ottersen OP (1998) Aquaporin-4 water channel protein in the rat retina and optic nerve: polarized expression in Muller cells and fibrous astrocytes. J Neurosci 18:2506-2519.

Nicholson C, Phillips JM (1981) Ion diffusion modified by tortuosity and volume fraction in the extracellular microenvironment of the rat cerebellum. J Physiol 321:225-257.

Nielsen S, Nagelhus EA, Amiry-Moghaddam M, Bourque C, Agre P, Ottersen OP (1997) Specialized membrane domains for water transport in glial cells: high-resolution immunogold cytochemistry of aquaporin-4 in rat brain. J Neurosci 17:171-180.

Olsson T, Broberg M, Pope KJ, Wallace A, Mackenzie L, Blomstrand F, Nilsson M, Willoughby JO (2006) Cell swelling, seizures and spreading depression: an impedance study. Neuroscience 140:505-515.

Ostby I, Oyehaug L, Einevoll GT, Nagelhus EA, Plahte E, Zeuthen T, Lloyd CM, Ottersen OP, Omholt SW (2009) Astrocytic mechanisms explaining neural-activity-induced shrinkage of extraneuronal space. PLoS Comput Biol 5:e1000272.

Skucas VA, Mathews IB, Yang J, Cheng Q, Treister A, Duffy AM, Verkman AS, Hempstead BL, Wood MA, Binder DK, Scharfman HE (2011) Impairment of select forms of spatial memory and neurotrophin-dependent synaptic plasticity by deletion of glial aquaporin-4. J Neurosci 31:6392-6397.

Sykova E, Nicholson C (2008) Diffusion in brain extracellular space. Physiol Rev 88:1277-1340.

Sykova E, Vargova L, Kubinova S, Jendelova P, Chvatal A (2003) The relationship between changes in intrinsic optical signals and cell swelling in rat spinal cord slices. Neuroimage 18:214-230.

Takano T, Tian GF, Peng W, Lou N, Lovatt D, Hansen AJ, Kasischke KA, Nedergaard M (2007) Cortical spreading depression causes and coincides with tissue hypoxia. Nat Neurosci 10:754-762.

Thrane AS, Rappold PM, Fujita T, Torres A, Bekar LK, Takano T, Peng W, Wang F, Thrane VR, Enger R, Haj-Yasein NN, Skare O, Holen T, Klungland A, Ottersen OP, Nedergaard M, Nagelhus EA (2011) Critical role of aquaporin-4 (AQP4) in astrocytic Ca2+ signaling events elicited by cerebral edema. Proc Natl Acad Sci U S A 108:846-851.

Uckermann O, Vargova L, Ulbricht E, Klaus C, Weick M, Rillich K, Wiedemann P, Reichenbach A, Sykova E, Bringmann A (2004) Glutamate-evoked alterations of glial and neuronal cell morphology in the guinea pig retina. J Neurosci 24:10149-10158.

Van HA, Khattab FI (1967) Changes in cortical extracellular space during spreading depression investigated with the electron microscope. J Neurophysiol 30:911-929.

Verkman AS, Binder DK, Bloch O, Auguste K, Papadopoulos MC (2006) Three distinct roles of aquaporin-4 in brain function revealed by knockout mice. Biochim Biophys Acta 1758:1085-1093.

Veruki ML, Wassle H (1996) Immunohistochemical localization of dopamine D1 receptors in rat retina. Eur J Neurosci 8:2286-2297.

Viitanen T, Ruusuvuori E, Kaila K, Voipio J (2010) The K+-Cl cotransporter KCC2 promotes GABAergic excitation in the mature rat hippocampus. J Physiol 588:1527-1540.

Voipio J, Pasternack M, MacLeod K (1994) Ion-sensitive microelectrodes. In: Microelectrode Techniques - The Plymouth Workshop Handbook (Ogden D, ed), pp 275-316. Cambridge: The Company of Biologists Limited

FIGURE LEGENDS

Figure 1. Distribution of AQP4 immunofluorescence in the mouse hippocampus. **(A)** AQP4 labeling (green) was found in multiple processes in stratum pyramidale (pyr) and stratum radiatum (rad) in acute hippocampal slices of wild-type mice. Co-immunostaining with antibodies against GFAP (**B**, red), and NeuN (**C**, blue) showed that AQP4 resided in astrocytes, including their delicate processes (arrowheads) that outlined pyramidal cell bodies (merged and enlarged image in **F**). Note the strong labeling of perivascular astrocytic endfeet (double arrowheads). AQP4 immunolabeling pattern of hippocampi from acute slices (**A**) and perfusion-fixed brain was comparable. Absence of AQP4 labeling in an acute hippocampal slice from *Aqp4*$^{-/-}$ mice (**E**) confirmed the selectivity of antibodies. Scale bars, 50 μm.

Figure 2. Distribution of AQP4 immunogold reactivity in the mouse hippocampus. Electron micrographs from wild-type (**A**-**C**) and *Aqp4*$^{-/-}$ (**D**-**F**) mice. (**A**) Gold particles signaling AQP4 decorate astrocytic processes (Ast, yellow) ensheating synapses in stratum radiatum. (**B**) Immunopositive astrocytic processes are seen in the tiny cleft between pyramidal (Pyr) cell somata. Arrowheads denote the pyramidal cell membrane. Box in inset displays the region shown at higher magnification in B. (**C**) High density of AQP4 labeling along astrocytic endfoot membranes abutting on a capillary endothelial cell (Cap). (**D-F**) Corresponding motifs to those in (A-C), but from *Aqp4*$^{-/-}$ mice. Lu, lumen. Scale bars, 0.2 μm and 2 μm (insets).

Figure 3. Impact of *Aqp4* gene deletion on ECS volume dynamics. ***A*,** Schematic drawing of a hippocampal slice showing the localization of the stimulating and the extracellular voltage

(V_o, green) and ion-sensitive recording (TMA^+, yellow) electrodes. Traces are representative synaptic responses (fEPSPs) elicited in stratum radiatum from WT (blue) and *Aqp4*$^{-/-}$ (red) mice. ***B*,** Representative traces of ECS volume dynamics in stratum radiatum before and during a 20 Hz stimulation train (1 min, black bar along the abscissa) in WT and *Aqp4*$^{-/-}$ mice. Note the different time scales along the abscissa. ***C*,** As in B, but data are pooled from 23 (WT) and 26 (*Aqp4*$^{-/-}$) slices and shown as mean ± SEM. Violet horizontal bar along the abscissa indicate $p < 0.05$ when comparing the genotypes. ***D*,** As in C, but the ECS volume dynamics have been recorded and measured in the stratum pyramidale in slices from WT (n = 9) and *Aqp4*$^{-/-}$ (n = 11) mice. Statistical analysis like in C did not detect $p < 0.05$ at any time point between the genotypes. The histogram shows a comparison of the changes in ECS volume in stratum radiatum (rad) and straum pyramidale (pyr) measured 10 s after the start of the stimulation train. Recordings were done both in stratum radiatum and stratum pyramidale in the same slices (WT, n = 6; *Aqp4*$^{-/-}$, n = 7 mice). * $p < 0.05$ (two-tailed paired t-test).

Figure 4. Impact of *Aqp4* deletion on excitatory synaptic transmission, excitability and synaptic plasticity in the hippocampal CA1 region. ***A*,** Stimulation strength (in nC) necessary to elicit prevolleys of 0.5, 1.0, and 1.5 mV. ***B*,** fEPSP amplitudes as a function of the same three prevolley amplitudes. ***C*,** The fEPSP amplitude necessary to elicit a just detectable population spike (1) and a population spike of 2 mV amplitude (2). ***D*,** Paired-pulse facilitation ratio (fEPSP2/fEPSP1) in the two genotypes at an interstimulus interval of 50 ms. Data are shown as mean ± SEM. ***E*,** Top traces: Means of five consecutive synaptic responses induced by different stimulation strengths recorded in stratum radiatum in slices from WT (left) and *Aqp4*$^{-/-}$ (right) mice. Prevolleys preceding the fEPSPs are indicated by a filled circle. Bottom traces: Means of five consecutive responses from stratum pyramidale elicited by paired-pulse stimulation (50 ms interstimulus interval) at different stimulation strengths.

Arrows indicate population spike threshold. ***F*,** Normalized and pooled fEPSP slope measurements during the first 30 s of a 20 Hz stimulation train in slices from WT (n = 21) and *Aqp4*$^{-/-}$ (n = 21) mice. **a** indicates the time point of the maximum amplitude of the intitial frequency facilitation, **b** the transition point between the initial frequency facilitation and the DRE, **c** the peak of the DRE. The histogram to the right depicts the mean time ± SEM needed to reach a (WT mice: 0.75 ± 0.06 s, n = 21 vs. *Aqp4*$^{-/-}$: 0.62 ± 0.06 s, n = 21), b (WT mice: 3.61 ± 0.12 s vs. *Aqp4*$^{-/-}$: 3.40 ± 0.12 s), and c (WT mice: 6.02 ± 0.21 s vs. *Aqp4*$^{-/-}$: 6.38 ± 0.20 s). The inset graph to the left shows normalized means of the baseline fEPSPs elicited by low frequency activation (0.1 Hz) prior to and just following the 20 Hz stimulation train (indicated by the black bar along the abscissa). ***G*,** Normalized fEPSP slopes evoked at CA3-to-CA1 synapses in slices from wild-type and *Aqp4*$^{-/-}$ mice from 10 min before to 50 min after tetanic stimulation. The tetanized pathways are shown as circles, the untetanized control pathways as triangles. Data are shown as mean ± SEM.

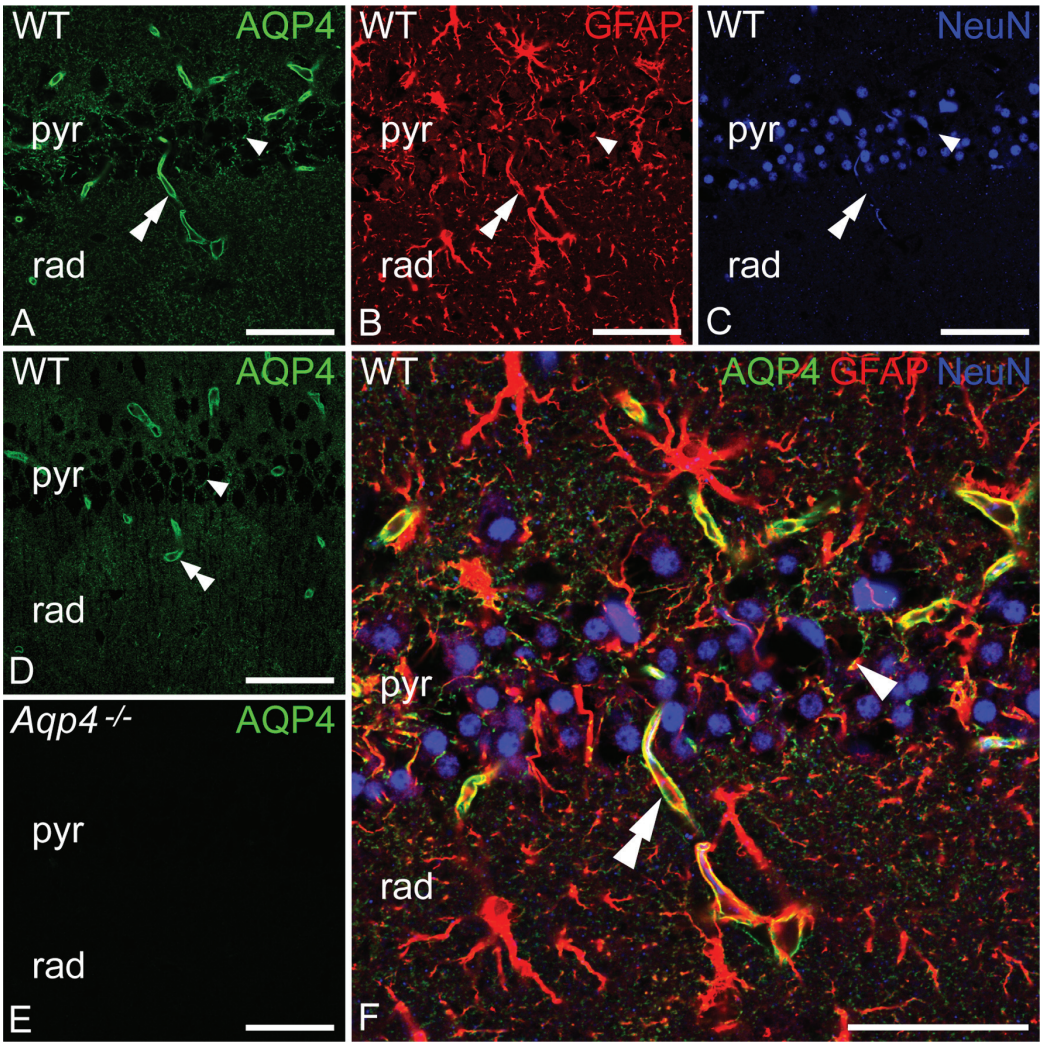
WT
AQP4
pyr
rad
A
WT
GFAP
pyr
rad
B
WT
NeuN
pyr
rad
C
WT
AQP4
pyr
rad
D
Aqp4 -/-
AQP4
pyr
rad
E
WT
AQP4 GFAP NeuN
pyr
rad
F

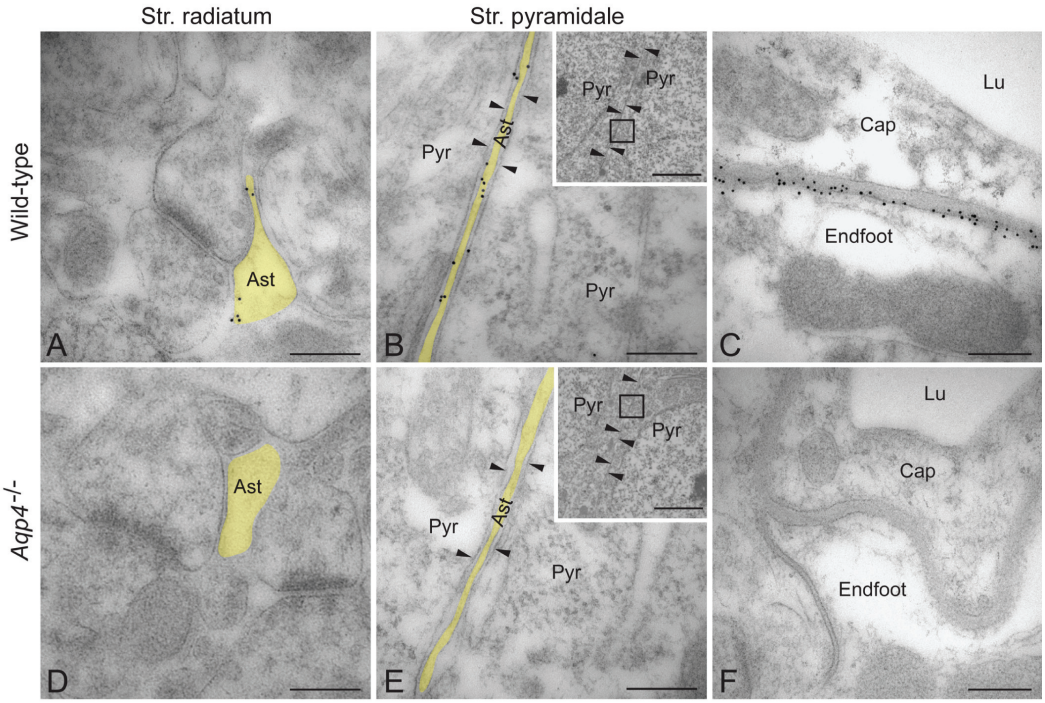
Str. radiatum
Str. pyramidale
Wild-type
Aqp4-/-
Ast
Pyr
Lu
Cap
Endfoot
A
B
C
D
E
F

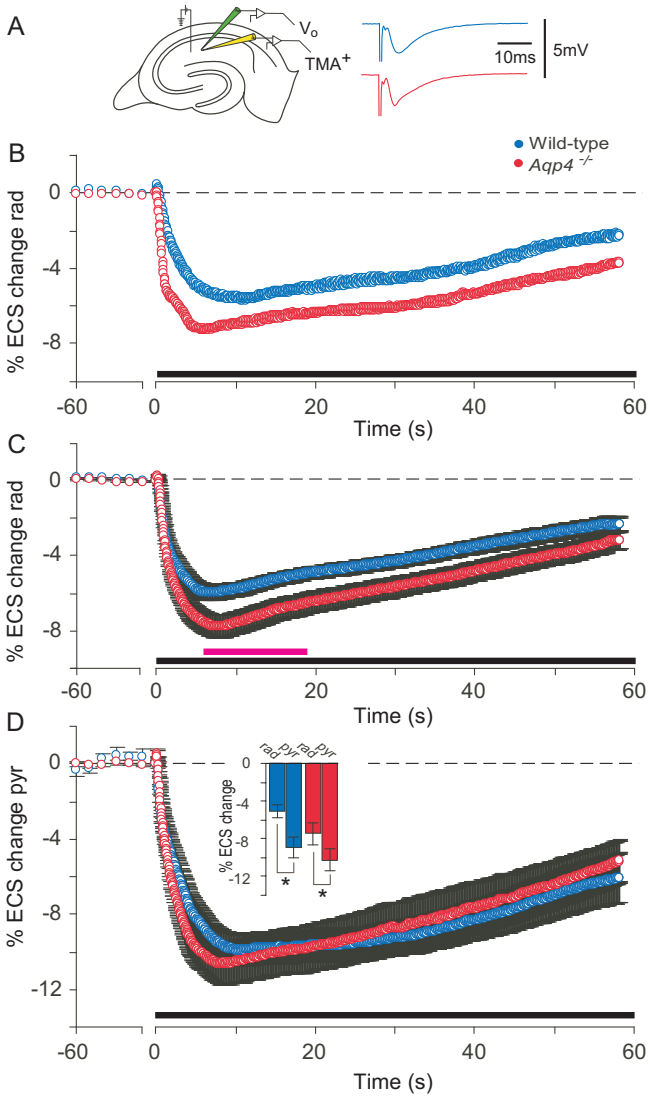
A
Vo
TMA+
10ms
5mV
B
Wild-type
Aqp4 -/-
% ECS change rad
0
-4
-8
-60
0
20
40
60
Time (s)
C
% ECS change rad
0
-4
-8
-60
0
20
40
60
Time (s)
D
% ECS change pyr
0
-4
-8
-12
-60
0
20
40
60
Time (s)
rad
pyr
rad
pyr
% ECS change
0
-4
-8
-12
*
*

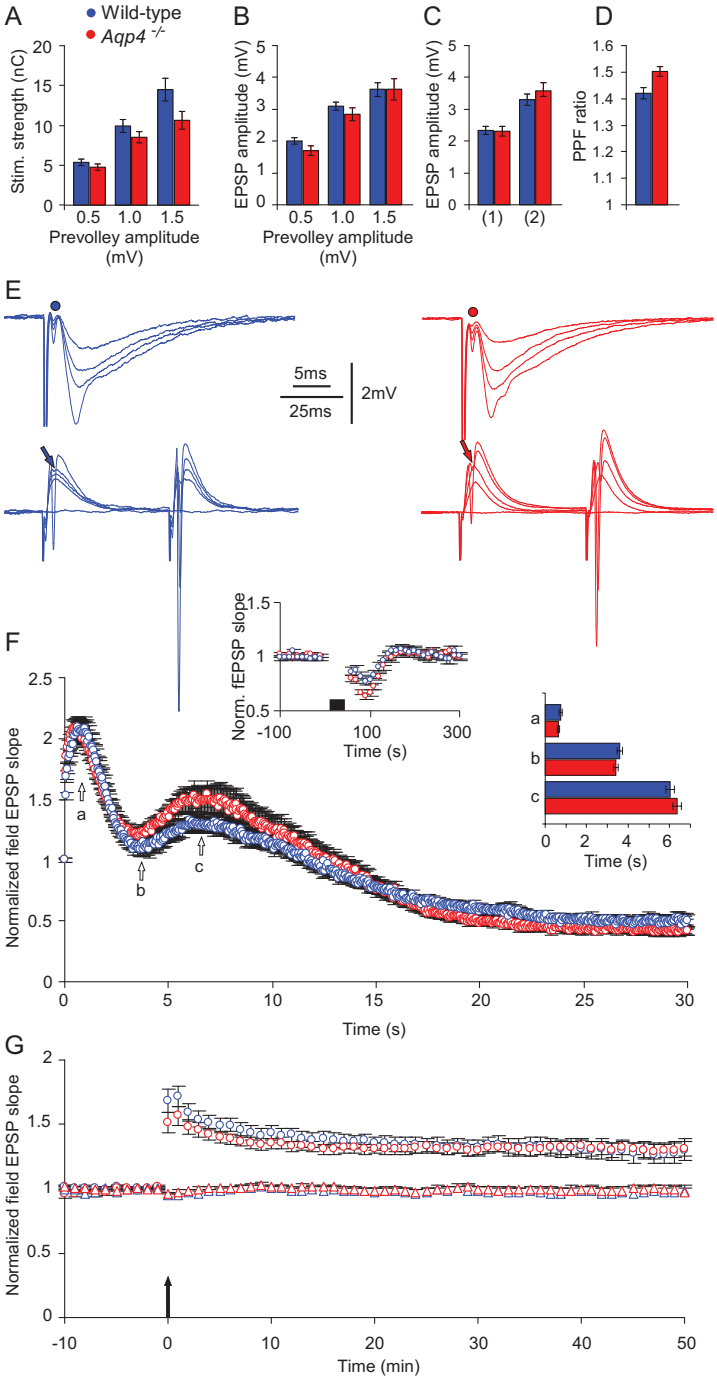
A
Wild-type
Aqp4 -/-
Stim. strength (nC)
Prevolley amplitude (mV)
B
EPSP amplitude (mV)
Prevolley amplitude (mV)
C
EPSP amplitude (mV)
(1)
(2)
D
PPF ratio
E
5ms
25ms
2mV
F
Norm. fEPSP slope
Time (s)
Normalized field EPSP slope
a
b
c
Time (s)
G
Normalized field EPSP slope
Time (min)

III

Deletion of aquaporin-4 changes the perivascular glial protein scaffold without disrupting the brain endothelial barrier

Martine Eilert-Olsen[1,2], Nadia Nabil Haj-Yasein[1,2], Gry Fluge Vindedal[1], Rune Enger[1,2], Georg Andreas Gundersen[1,2], Eystein Hellstrøm Hoddevik[2], Pétur Henry Petersen[3], Finn-Mogens S. Haug[2], Øivind Skare[4], Marvin E. Adams[5], Stanley C. Froehner[5], John Michael Burkhardt[1], Anna E. Thoren[1,2], and Erlend A. Nagelhus[1,2,6*]

[1]Centre for Molecular Medicine Norway, Nordic EMBL Partnership, University of Oslo, P.O. Box 1137 Blindern, N-0318 Oslo, Norway.

[2]Centre for Molecular Biology and Neuroscience, Institute of Basic Medical Sciences, University of Oslo, P.O. Box 1105 Blindern, 0317 Oslo, Norway.

[3]Biomedical Center, Department of Anatomy, Faculty of Medicine, University of Iceland, 101 Reykjavík, Iceland.

[4]Division of epidemiology, Norwegian Institute of Public Health, 0403 Oslo, Norway, and Department of Public Health and Primary Health Care, University of Bergen, 5020 Bergen, Norway.

[5]Department of Physiology and Biophysics, University of Washington, Seattle, Washington 98195, USA.

[6]Oslo University Hospital, Department of Neurology, 0027 Oslo, Norway.

Running title: *Aqp4* deletion alters endfoot protein scaffold

Number of words by section: 172 in Abstract, 391 in Introduction, 1543 in Materials and Methods, 483 in Results, 808 in Discussion (including Acknowledgments), 813 in Figure Legends, 1360 in References

Number of figures: 4

Number of tables: 0

Total word count: 5578 (previous version was 6339)

Number of pages: 26

*Correspondence to: Erlend A. Nagelhus, MD, PhD, Centre for Molecular Medicine Norway, Nordic EMBL Partnership, University of Oslo, P.O. Box 1137 Blindern, 0318 Oslo, Norway. Phone: +47 91736316. E-mail: e.a.nagelhus@ncmm.uio.no

Key Words: AQP4, astrocytes, blood-brain barrier, endfeet, syntrophin

Abbreviations: AQP4, aquaporin-4; BBB, blood-brain barrier; DAPC, dystrophin-associated protein complex; PB, phosphate buffer; WT, wild-type

ABSTRACT

Expression of the water channel aquaporin-4 (AQP4) at the blood-brain interface is dependent upon the dystrophin associated protein complex. Here we investigated whether deletion of the *Aqp4* gene affects the molecular composition of this protein scaffold and the integrity of the blood-brain barrier. High-resolution immunogold cytochemistry revealed that perivascular expression of α-syntrophin was reduced by 60% in *Aqp4*$^{-/-}$ mice. Additionally, perivascular AQP4 expression was reduced by 88% in *α-syn*$^{-/-}$ mice, in accordance with earlier reports. Immunofluorescence showed that *Aqp4* deletion also caused a modest reduction in perivascular dystrophin, whereas β-dystroglycan labeling was unaltered. Perivascular microglia were devoid of AQP4 immunoreactivity. Deletion of *Aqp4* did not alter the ultrastructure of capillary endothelial cells, the expression of tight junction proteins (claudin-5, occludin and zonula occludens 1), or the vascular permeability to horseradish peroxidase and Evans blue albumin dye. We conclude that *Aqp4* deletion reduces the expression of perivascular glial scaffolding proteins without affecting the endothelial barrier. Our data also indicate that AQP4 and α-syntrophin are mutually dependent upon each other for proper perivascular expression.

INTRODUCTION

The water channel aquaporin-4 (AQP4) is abundant at the brain-blood interface (Frigeri et al, 1995; Nielsen et al, 1997), and studies using knockout mice have shown that it has dramatic impact on development and resolution of brain edema in various disease models (Manley et al., 2000; Amiry-Moghaddam et al., 2003; Papadopoulos et al., 2005; Bloch et al., 2005; Bloch et al., 2006; Haj-Yasein et al., 2011a). Thus, AQP4 has emerged as a promising target for novel treatment strategies of brain edema (Papadopoulos and Verkman, 2008). However, the possibility that deletion of the *Aqp4* gene has secondary effects on brain microvessel structure and function must be considered.

Anchoring of AQP4 in perivascular astrocytic endfeet is mediated by the dystrophin-associated protein complex (DAPC) (Frigeri et al., 2001; Neely et al., 2001). Notably, deletion of α-syntrophin, a component of the dystrophin-based protein scaffold, leads to a 90% reduction of AQP4 expression in astrocytic endfeet (Neely et al., 2001). In several dystrophin-deficient mouse mutants, the decreased perivascular AQP4 level is associated with altered ultrastructure and integrity of the blood-brain barrier (BBB) (Nicchia et al., 2004; Nico et al., 2003; Vajda et al., 2002). The BBB depends on the physical barrier formed by endothelial tight junctions and a transport barrier resulting from membrane transporters, enzymes and vesicular mechanisms (Abbott et al., 2010). While maturation of the BBB is correlated with AQP4 expression (Wen et al., 1999; Nicchia et al., 2004), breakdown of the BBB is associated with increased expression of AQP4 (Saadoun et al., 2002; Taya et al., 2010).

Previous work has shown that AQP4-deficient CD1 mice exhibit open endothelial tight junctions, swollen astrocytic endfeet, and hyperpermeability of the BBB (Zhou et al.,

2008). However, in more recent studies, *Aqp4* deletion did not affect capillary ultrastructure and BBB permeability for horseradish peroxidase (HRP) (Saadoun et al., 2009) or Evans Blue (Feng et al., 2009). The aim of this study was to use a different line of *Aqp4*$^{-/-}$ mice, backcrossed on the C57BL/6J background, to resolve whether *Aqp4* gene deletion perturbs the organization of the perivascular astrocytic protein scaffold and, if so, whether this perturbation affects BBB permeability and expression of tight junction proteins. These questions are critical for an appropriate understanding of the functional role of AQP4 in the CNS and for a correct interpretation of the physiological and pathophysiological effects observed after *Aqp4* gene deletion.

MATERIALS AND METHODS

Animals

Aqp4$^{-/-}$ mice backcrossed to a C57BL/6J background for 5 generations (Thrane et al., 2011), wild-type (WT) mice of same genetic background, and α-syntrophin$^{-/-}$ mice (Adams et al., 2000) were used. Studies were conducted with mice aged 8-12 weeks, weighing 20-30g. All experiments were approved by the University of Oslo's Animal Care and Use Committee.

Primary antibodies

We used rabbit affinity-purified polyclonal antibodies against α-syntrophin (Syn259) (Peters et al., 1997), dystrophin (Dys331) (Kramarcy et al., 1994), AQP4 (Millipore and Sigma), β-

dystroglycan (Novocastra), claudin-5 (Invitrogen Corporation, Camarillo, CA, USA), occludin (Invitrogen Corporation), zonula occludens 1 (ZO-1; ProteinTech Group, Chicago, IL, USA), and β-actin (Abcam, Saint Louis, MO, USA), mouse monoclonal antibodies against GFAP (Millipore, Cat# MAB 360), goat polyclonal antibodies against IBA1 (Abcam, Saint Louis, MO, USA), and rat monoclonal antibodies against CD31 (BD Bioscience Pharmingen).

Immunocytochemistry

For all fixation protocols, the animals were deeply anesthetized with a mixture of chloral hydrate, magnesium sulphate and pentobarbital (142, 70 and 32 mg/kg body weight i.p., respectively) before transcardiac perfusion with 0.1 M phosphate buffer (PB; pH 7.4) with 2% dextran for 15-20 sec and fixative for 20-30 min (flow rate ~8ml/min). For α-syntrophin immunogold cytochemistry, 5 *Aqp4*$^{-/-}$, 5 WT, and 3 *α-syn*$^{-/-}$ animals were fixed using 4% formaldehyde in PB containing 0.2% picric acid at pH 6.0, followed by a similar fixative at pH 10.0 ("pH-shift" protocol; as described by Nagelhus et al., 1998). For AQP4 immunogold cytochemistry, 7 WT and 8 *α-syn*$^{-/-}$ animals were fixed using 4% formaldehyde in PB containing 0.1% glutaraldehyde. For immunofluorescence, at least 3 mice of each genotype were fixed with 4% formaldehyde in PB, and for morphological analysis 5 *Aqp4*$^{-/-}$ and 4 WT mice were fixed with 2.5% glutaraldehyde and 1% formaldehyde in PB.

Light microscopic immunocytochemistry

The perfused animals were stored at 4^{o} C overnight. The brain was removed and cryoprotected in sucrose (10%, 20% and 30% in PB), and sections were cut at 15 μm on a cryostat. Light microscopic immunocytochemistry was carried out using an indirect

fluorescence method (Nagelhus et al., 1998). The concentrations of antibodies were: anti-AQP4, 2 μg/ml (Milipore) and 3 μg/ml (Sigma); anti-GFAP, 1:500 of stock solution; anti-IBA1, 5 μg/ml; anti-α-syntrophin, 1.2 μg/ml; anti-dystrophin, 6 μg/ml; anti-β-dystroglycan, 0.46 μg/ml; anti-rat CD31, 2.5 μg/ml. The primary antibodies were revealed by donkey secondary antibodies with indocarbocyanine (Cy3), indodicarbocyanine (Cy5) or Alexa Fluor 488 (1:1,000: Jackson ImmunoResearch Laboratories, Inc., West Grove, PA). Cortical sections were viewed and photographed with a Zeiss LSM 5 PASCAL microscope equipped with epifluorescence optics, using filter BP 505-530, LP 560 and LP 650, and objective 20X/0.75 Plan-Apochromat, 40X/1.3 Oil Plan-Neofluar, or 63X/1.40 Oil Plan-Apochromat.

Electron microscopic immunocytochemistry and morphological analysis

Small blocks of fixed cortex were subjected to freeze substitution as described previously (Nagelhus et al., 1998). Ultrathin sections were cut with a Reichert ultramicrotome, mounted on nickel grids, and processed for immunogold cytochemistry as described previously (Nagelhus et al., 1998). Briefly, sections were incubated sequentially in the following solutions (at room temperature): (1) 50 mM glycine in Tris buffer (5 mM) containing 0.01% Triton X-100 and 50mM NaCl (TBST; 10 min); (2) 0.2% milk powder in TBST (10 min); (3) primary antibody (anti-AQP4 from Sigma, 1.5 μg/ml and anti-α-syntrophin, 12 μg/ml) diluted in the solution used in the preceding step (overnight); (4) same solution as in step 2 (10 min x 2); (5) gold-conjugated IgG (GAR10 nm; Abcam), diluted 1:20 in TBST containing milk powder and polyethylene glycol (0.5 mg/ml, 1 h). Finally, the sections were counterstained and examined in a Fei Tecnai 12 transmission electron microscope. For morphological analysis, ultrathin sections were only counterstained and examined.

Detection and quantification of gold particles. The analyzer was blind to genotype.

Digital images were acquired with a commercially available image analysis program (analySIS" Soft Imaging Systems GmbH, Münster, Germany), modified for acquisition of high-resolution digital images and semiautomatic evalution of immunogold-labeled cellular volumes and surfaces (membranes). For purposes of the study, images of membrane segments were recorded at a nominal magnification of x43000, in 2048 x 2048 x 8 bit images. One section from each animal was analyzed. In each section, 14-15 capillaries were identified, and 1-3 images of perivascular astrocytic endfoot membrane segments were acquired from each capillary. Gold particles in proximity to each membrane-curve were detected semiautomatically, and the distance between each particle's centre of gravity and its membrane curve was calculated by the program. Particles localized within 21 nm from their membrane curve were included in the automated calculation of the number of particles per unit length of membrane (linear particle density) (Nagelhus et al., 1998). Membrane segments from the same capillary were aggregated. All images, with associated curves and particles, were saved with the measurements, to allow later verification and correction. The measurements were exported to the SPSS 16.0 for Windows software package (SPSS Inc, Chicago, IL, USA), for survey and quality control.

Statistical analysis of immunogold data. An ordinary linear regression model assumes that all observations are independent, an assumption which is not valid for our data since we have multiple observations for each animal. We used instead a linear mixed model which takes into account the dependency between observations from the same animal, by including two variance terms, one for between-animal variation and one for within-animal variation. For statistical analysis of this model we used the R function lme in the nlme package (Pinheiro JC and Bates DM, 2000) which gives us estimated differences in linear particle density between genotypes and corresponding P-values. We examined different transformations of Y_{ij} and found that a log transformation gave the best fit to the normal distribution, as seen by a

quantile-quantile plot. In the analysis, we thus used log-transformed observations. The animals were divided into groups of different genotypes (*Aqp4*$^{-/-}$, WT and *α-syn*$^{-/-}$). The linear densities (log transformed) were modeled by a linear mixed model $Y_{ij} = \mu + \beta g_i + u_i + w_{ij}$. Here, Y_{ij} is the log-transformed measurement of the linear density for animal i and repetition (membrane segment) j, g_i is the genotype of animal i, and μ and βg are fixed effects, where μ represents the reference genotype (*Aqp4*$^{-/-}$ or *α-syn*$^{-/-}$, depending on the analysis) and βg represents the difference between genotypes. The random effect u_i represents variation between animals and the random effect w_{ij} represents variation within animals. The terms u_i and w_{ij} are normally distributed with means 0 and variances σ_u^2 and σ_{w,g_i}^2, respectively. In the linear mixed model we allowed the variance σ_{w,g_i}^2 to vary between genotypes. The chosen model structure was based on likelihood ratio tests. The fixed effects were estimated by maximum likelihood and the variances of the random effects were estimated by restricted maximized likelihood (Cnaan et al., 1997).

HRP staining

To investigate the comparative BBB permeability of WT and *Aqp4*$^{-/-}$ mice, a HRP assay of cortical vessels was performed as described previously (Nico et al., 2003; Zhou et al., 2008), with some modifications. HRP (Sigma, Saint Louis, Missouri, USA; 0.3mg/g body weight in 0.1ml saline solution) was injected into the tail vein of anesthetized *Aqp4*$^{-/-}$ and WT adult male mice (8-24 weeks; n = 2, respectively) maintained at 37^{o}C on a heating pad. After 10 min they were decapitated, and their brains were fixed by immersion fixation in 4% formaldehyde for 48 hours. Cortical sections were cut to 50μm with a vibratome and incubated for 30 minutes at room temperature in a 0.05% solution of diaminobenzidine (DAB) in 0.05M Tris-HCl buffer (pH=7.6) containing 0.01% H_2O_2. Images were taken from

the parietal cortex with a Colour View camera (Soft Imaging Systems, Olympus) on an Olympus BX51 microscope using UPlanFI 10x/0.30 and UPlanApo 60x/0.90 objectives.

Evans blue analysis

Quantitative analysis of BBB permeability was performed using a spectrophotometry protocol with the Evans blue albumin dye, as decribed previously (Haj-Yasein et al., 2011a). Subject groups consisted of 8 male WT mice and 8 male *Aqp4*$^{-/-}$ mice. Mice were between 10 and 18 weeks old, and weighed between 20 and 32 grams.

Statistical analyses. Normalized Evans blue content values were compared using a one-way ANOVA. Post-hoc analysis was performed via a Bonferroni test. All statistical comparisons were performed using the SPSS 17.0 for Windows software package (SPSS Inc, Chicago, IL, USA). Significance was taken at $p<0.05$. All data are presented as mean ± standard error.

Western blotting

After homogenization and solubilization, extracts of mouse brain (sample with 10 µg protein for ZO-1 and occludin, 30 µg for claudin-5) were loaded onto precast 7.5% Criterion SDS/PAGE gels for the ZO-1 blots, onto precast 10% Criterion SDS/PAGE gels for the occludin blots, and onto precast "Any kD" Mini-protean TXG SDS/PAGE gels for the claudin-5 blots (all from Bio-Rad), then subsequently transferred onto a PVDF membrane from Bio-Rad , as described previously (Haj-Yasein et al., 2011b). The membranes were probed with rabbit-anti claudin-5 (5 µg/ml), rabbit-anti occludin (3 µg/ml) and rabbit-anti-ZO-1 antibody (0.8 µg/ml), followed by alkaline phosphatase-conjugated rabbit-anti-goat IgG (1:10.000). Blots were developed by using the ECF fluorescent substrate (GE Healthcare) and

visualized on a Typhoon 9410 scanner (Amersham). The membranes were stripped, and reprobed with rabbit-anti-β-actin (1.3 μg/ml) for loading control.

Densitometry was done by the gel analysis tool built into the ScienceLinker (Oslo, Norway) database system. The extracted data were analyzed using GraphPad Prism 4 (Graph-Pad Software Inc., San Diego, CA, USA).

RESULTS

Immuncytochemical analysis of the perivascular glial protein scaffold

In agreement with earlier reports, AQP4 immunofluorescence was found in GFAP-labeled astrocytes, with the most distinct signal in perivascular endfeet (Fig. 1A-C). IBA1-immunopositive microglial cells were without detectable AQP4 labeling (Fig. 1D-F). The strongest immunoreactivity for dystrophin, α-syntrophin, and β-dystroglycan was found around cortical vessels (Fig.1G-I). Deletion of *Aqp4* profoundly reduced perivascular α-syntrophin labeling (Fig. 1J), and caused a modest reduction in dystrophin labeling (Fig. 1K). These changes were evident for vessels of all calibers. The staining for β-dystroglycan was similar in the two genotypes (Fig. 1I,L).

High-resolution immunogold cytochemistry on brain tissue fixed for optimal preservation of antigenicity ("pH-shift fixation protocol") showed that α-syntrophin was present on astrocytic membranes abutting cortical capillaries of WT mice (Fig. 2A). When assessing the distribution of gold particles along an axis perpendicular to the plasma membrane, we found a peak corresponding to the astrocytic plasma membrane and its immediate cytoplasmic vicinity (inset in Fig. 2A), corresponding to the localization of α-

syntrophin. The peak was absent in *α-syn*$^{-/-}$ mice, confirming the selectivity of the antibodies (inset in Fig. 2C).

In *Aqp4*$^{-/-}$ mice, gold particles indicating α-syntrophin still clustered over the plasma membrane, but were less abundant (Fig. 2B). Quantitative analysis revealed that the perivascular immunogold signal for α-syntrophin was reduced by ~60% in *Aqp4*$^{-/-}$ mice compared to WT (Fig. 2E; $p<0.001$, mixed model statistical analysis, cf. Materials and Methods). Non-specific immunogold labeling was assessed in adjacent ultrathin sections from *α-syn*$^{-/-}$ mice and amounted to <7% of the signal in WTs (0.17±0.03, n=45 vs. 2.74±0.15, n=74, respectively; $p<0.001$, not illustrated).

To demonstrate that AQP4 and α-syntrophin are dependent upon each other for proper perivascular expression, we performed a quantitative analysis of AQP4 immunogold reactivity in WT and in *α-syn*$^{-/-}$ mice. Deletion of *α*-syntrophin caused an 88% reduction of AQP4 immunogold signal in astrocytic endfeet (Fig. 2D-F), in agreement with a previous report (Neely et al., 2001).

Ultrastructural architecture of brain capillaries and blood-brain barrier permeability

Electron microscopy of brain sections from WT and from *Aqp4*$^{-/-}$ mice fixed with 2.5% glutaraldehyde and 1% formaldehyde showed cerebral capillaries of indistinguishable morphology (Fig. 3). Notably, pericytes and endothelial tight junctions were present in both genotypes, and the area covered by astrocytic endfeet was apparently similar (Fig. 3).

In line with the normal BBB morphology, qualitative and quantitative assessment of barrier permeability with HRP and Evans blue albumin dye, respectively, showed no differences between genotypes (Fig. 4A-E). Thus, HRP signal was confined to the vasculature

in both WT (Fig. 4A) and *Aqp4*$^{-/-}$ mice (Fig. 4B), and neither genotype showed visible blue coloration of the brain after systemic injection of Evans blue (Fig. 4C, D). Evans blue content was calculated from the recorded spectrophotometric absorption and %-transmission values at 590 nm and reported as µg Evans blue per gram of brain mass (Fig. 4E). No difference was found between WT and *Aqp4*$^{-/-}$ mice (Fig. 4E).

DISCUSSION

It is widely accepted that AQP4 plays a role in maintaining water homeostasis at the blood-brain barrier (Amiry-Moghaddam and Ottersen, 2003). The seminal discovery that *Aqp4* gene deletion protects against brain edema in experimental stroke (Manley et al., 2000) was followed by studies showing that depletion of AQP4-anchoring molecules had similar effects (Vajda et al., 2002; Amiry-Moghaddam et al., 2003). However, the possibility must be considered that molecules other than perivascular AQP4 contribute to the observed phenotype of these mutant mice.

Perivascular expression of AQP4 is contingent upon dystrophin (Frigeri et al., 2001) and α-syntrophin (Neely et al., 2001), two components of the DAPC. α-Syntrophin emerges as the central organizer of the astrocyte DAPC, given that its absence results in loss of other DAPC molecules (Bragg et al., 2010). α-Syntrophin also interacts with the inwardly-rectifying K^+ channel Kir4.1 (Connors et al., 2004) and the β_1 subunit of the Na-K-ATPase (Brignone et al., 2010). Both Kir4.1 and the sodium pump have substantial impact on CNS water homeostasis (Dibaj et al., 2007; Fort et al., 2008; Leis et al., 2005; Mintorovitch et al., 1994).

Here we show that *Aqp4* gene deletion modulates the astrocytic protein scaffold around capillaries. We found that deletion of *Aqp4* reduced the level of α-syntrophin immunogold signal in astrocytic endfeet by 60%, and conversely, deletion of α-syntrophin caused an 88% reduction in perivascular AQP4 immunogold labeling, in agreement with a previous report (Neely et al., 2001). Thus, AQP4 and α-syntrophin are mutually dependent upon each other for proper expression in astrocytic endfeet. Moreover, deletion of *Aqp4* caused a reduction of perivascular dystrophin, as also found in *α-syn*$^{-/-}$ mice (Bragg et al., 2006).

One possible mechanism underlying the interdependency between AQP4 and anchoring molecules is that both AQP4 and scaffolding proteins are assembled into a vesicular complex before transportation to astrocytic endfeet, as proposed for DAPC (Bragg et al., 2010). Alternatively, the stability of the molecules in the endfeet may depend upon their interaction.

The interdependency of AQP4 and DAPC molecules was only partial, as 40% of perivascular α-syntrophin remained after *Aqp4* deletion, as did most of the dystrophin. However, expression of β-dystroglycan did not seem to be contingent upon AQP4.

Since microglial cells are a component of the perivascular glia limitans (Lassmann et al., 1991) we assessed whether microglia express AQP4. We found no AQP4 immunoreactivity in microglia, in line with a previous report (Li et al., 2011). Moreover, we recently failed to detect remaining AQP4 in brains of conditional *Aqp4* knockout mice where Cre recombinase was driven by *GFAP,* a promoter not expressed by microglia (Haj-Yasein et al., 2011a).

Recently it was shown that BBB permeability depends on pericytes (Daneman et al., 2010; Armulik et al., 2010), and that AQP4 polarization is perturbed in pericyte-deficient

mice (Armulik et al., 2010). Reports conflict as to whether AQP4 modulates BBB integrity (Zhou et al., 2008; Saadoun et al., 2009; Feng et al., 2009). Our electron microscopic analysis confirmed the presence of pericytes and endothelial tight junctions in *Aqp4* mutant mice, and immunoblots revealed comparable levels of the tight junction proteins claudin-5, occludin and ZO-1 in the two genotypes. Moreover, using HRP and Evans Blue extravasation techniques, we found no evidence for BBB hyperpermeability in AQP4-deficient mice. Our results were obtained in C57BL/6J mice and are in agreement with those obtained in CD1 mice by Saadoun et al. (2009), but contrast those of Zhou et al. (2008), also using CD1 mice. Notably, the former group failed to replicate BBB dysfunction in the mouse strain used by Zhou et al. (Feng et al., 2009). Moreover, BBB permeability was found to be normal in *α-syn*$^{-/-}$ mice (Zeynalov et al., 2008). Taken together, there is little support for the hypothesis that AQP4 plays a major role in maintaining BBB integrity.

In muscle, the DAPC both provides mechanical stability and anchors molecules engaged in signaling (Blake et al., 2002). The dystrophin-based anchoring scaffold and AQP4 likely serve similar functions at the glio-vascular interface. In agreement, we have recently found that *Aqp4* deletion interferes with astrocytic ATP release and Ca^{2+} signaling during osmotic stress (Thrane et al., 2011). The perivascular protein scaffold might also provide structural stability for vessels and influence vascular dynamics.

Conclusion

We have shown that *Aqp4* deletion alters the molecular composition of the perivascular astrocytic protein scaffold. Loss of glial endfoot scaffolding proteins must be taken into consideration when interpreting phenotypic characteristics of *Aqp4* knockout mice.

ACKNOWLEDGMENTS

We thank Mrs. Bjørg Rieber, Mrs. Karen Marie Gujord, Mrs. Jorunn Knutsen, Mrs. Carina V. S. Knudsen, Mr. Gunnar F. Lothe, and dr. techn. P. Johannes Helm for expert technical assistance, and Professor Ole Petter Ottersen for valuable comments on the paper. This work was supported by the US National Institutes of Health (grants NIH grant NS33145 to S.C.F.), the Research Council of Norway (NevroNor, and FUGE grants), and by the Letten Foundation.

REFERENCES

Abbott NJ, Patabendige AA, Dolman DE, Yusof SR, Begley DJ. 2010. Structure and function of the blood-brain barrier. Neurobiol Dis 37:13-25.

Adams ME, Kramarcy N, Krall SP, Rossi SG, Rotundo RL, Sealock R, Froehner SC. 2000. Absence of alpha-syntrophin leads to structurally aberrant neuromuscular synapses deficient in utrophin. J Cell Biol 150:1385-1398.

Amiry-Moghaddam M, Otsuka T, Hurn PD, Traystman RJ, Haug FM, Froehner SC, Adams ME, Neely JD, Agre P, Ottersen OP, Bhardwaj A. 2003. An alpha-syntrophin-dependent pool of AQP4 in astroglial end-feet confers bidirectional water flow between blood and brain. Proc Natl Acad Sci U S A 100:2106-2111.

Amiry-Moghaddam M, Ottersen OP. 2003. The molecular basis of water transport in the brain. Nat Rev Neurosci 4:991-1001.

Armulik A, Genove G, Mae M, Nisancioglu MH, Wallgard E, Niaudet C, He L, Norlin J, Lindblom P, Strittmatter K, Johansson BR, Betsholtz C. 2010. Pericytes regulate the blood-brain barrier. Nature 468:557-561.

Blake DJ, Weir A, Newey SE, Davies KE. 2002. Function and genetics of dystrophin and dystrophin-related proteins in muscle. Physiol Rev 82:291-329.

Bloch O, Auguste KI, Manley GT, Verkman AS. 2006. Accelerated progression of kaolin-induced hydrocephalus in aquaporin-4-deficient mice. J Cereb Blood Flow Metab 26:1527-1537.

Bloch O, Papadopoulos MC, Manley GT, Verkman AS. 2005. Aquaporin-4 gene deletion in mice increases focal edema associated with staphylococcal brain abscess. J Neurochem 95:254-262.

Bragg AD, Amiry-Moghaddam M, Ottersen OP, Adams ME, Froehner SC. 2006. Assembly of a perivascular astrocyte protein scaffold at the mammalian blood-brain barrier is dependent on alpha-syntrophin. Glia 53:879-890.

Bragg AD, Das SS, Froehner SC. 2010. Dystrophin-associated protein scaffolding in brain requires alpha-dystrobrevin. Neuroreport 21:695-699.

Brignone MS, Lanciotti A, Macioce P, Macchia G, Gaetani M, Aloisi F, Petrucci TC, Ambrosini E. 2010. The {beta}1 subunit of the Na,K-ATPase pump interacts with megalencephalic leucoencephalopathy with subcortical cysts protein 1 (MLC1) in brain astrocytes: new insights into MLC pathogenesis. Hum Mol Genet.

Cnaan A, Laird NM, Slasor P. 1997. Using the general linear mixed model to analyse unbalanced repeated measures and longitudinal data. Stat Med 16:2349-2380.

Connors NC, Adams ME, Froehner SC, Kofuji P. 2004. The potassium channel Kir4.1 associates with the dystrophin-glycoprotein complex via alpha-syntrophin in glia. J Biol Chem 279:28387-28392.

Daneman R, Zhou L, Kebede AA, Barres BA. 2010. Pericytes are required for blood-brain barrier integrity during embryogenesis. Nature 468:562-6

Dibaj P, Kaiser M, Hirrlinger J, Kirchhoff F, Neusch C. 2007. Kir4.1 channels regulate swelling of astroglial processes in experimental spinal cord edema. J Neurochem 103:2620-2628.

Feng X, Papadopoulos MC, Liu J, Li L, Zhang D, Zhang H, Verkman AS, Ma T. 2009. Sporadic obstructive hydrocephalus in Aqp4 null mice. J Neurosci Res 87:1150-1155.

Fort PE, Sene A, Pannicke T, Roux MJ, Forster V, Mornet D, Nudel U, Yaffe D, Reichenbach A, Sahel JA, Rendon A. 2008. Kir4.1 and AQP4 associate with Dp71- and utrophin-DAPs complexes in specific and defined microdomains of Muller retinal glial cell membrane. Glia 56:597-610.

Frigeri A, Gropper MA, Umenishi F, Kawashima M, Brown D, Verkman AS. 1995. Localization of MIWC and GLIP water channel homologs in neuromuscular, epithelial and glandular tissues. J Cell Sci 108 (Pt 9):2993-3002.

Frigeri A, Nicchia GP, Nico B, Quondamatteo F, Herken R, Roncali L, Svelto M. 2001. Aquaporin-4 deficiency in skeletal muscle and brain of dystrophic mdx mice. FASEB J 15:90-98.

Haj-Yasein NN, Vindedal GF, Eilert-Olsen M, Gundersen GA, Skare Ø, Laake P, Klungland A, Thoren AE, Burkhardt JM, Ottersen OP, and Nagelhus EA. 2011a Glial-conditional deletion of *Aqp4* reduces blood-brain water uptake and confers barrier function on perivascular astrocyte endfeet. Proc Natl Acad Sci USA 108(43):17815-20.

Haj-Yasein NN, Jensen V, Vindedal GF, Gundersen GA, Klungland A, Ottersen OP, Hvalby O, Nagelhus EA. 2011b. Evidence that compromised K(+) spatial buffering contributes to the epileptogenic effect of mutations in the human kir4.1 gene (KCNJ10). Glia 59:1635-1642.

Kramarcy NR, Vidal A, Froehner SC, Sealock R. 1994. Association of utrophin and multiple dystrophin short forms with the mammalian M(r) 58,000 dystrophin-associated protein (syntrophin). J Biol Chem 269:2870-2876.

Lassmann H, Zimprich F, Vass K, Hickey WF. 1991. Microglial cells are a component of the perivascular glia limitans. J Neurosci Res 28:236-243.

Leis JA, Bekar LK, Walz W. 2005. Potassium homeostasis in the ischemic brain. Glia 50:407-416.

Li L, Zhang H, Varrin-Doyer M, Zamvil SS, Verkman AS. 2011. Proinflammatory role of aquaporin-4 in autoimmune neuroinflammation. FASEB J 25:1556-1566.

Manley GT, Fujimura M, Ma T, Noshita N, Filiz F, Bollen AW, Chan P, Verkman AS. 2000. Aquaporin-4 deletion in mice reduces brain edema after acute water intoxication and ischemic stroke. Nat Med 6:159-163.

Mintorovitch J, Yang GY, Shimizu H, Kucharczyk J, Chan PH, Weinstein PR. 1994. Diffusion-weighted magnetic resonance imaging of acute focal cerebral ischemia: comparison of signal intensity with changes in brain water and Na+,K(+)-ATPase activity. J Cereb Blood Flow Metab 14:332-336.

Nagelhus EA, Veruki ML, Torp R, Haug FM, Laake JH, Nielsen S, Agre P, Ottersen OP. 1998. Aquaporin-4 water channel protein in the rat retina and optic nerve: polarized expression in Muller cells and fibrous astrocytes. J Neurosci 18:2506-2519.

Neely JD, Amiry-Moghaddam M, Ottersen OP, Froehner SC, Agre P, Adams ME. 2001. Syntrophin-dependent expression and localization of Aquaporin-4 water channel protein. Proc Natl Acad Sci U S A 98:14108-14113.

Nicchia GP, Nico B, Camassa LM, Mola MG, Loh N, Dermietzel R, Spray DC, Svelto M, Frigeri A. 2004. The role of aquaporin-4 in the blood-brain barrier development and integrity: studies in animal and cell culture models. Neuroscience 129:935-945.

Nico B, Frigeri A, Nicchia GP, Corsi P, Ribatti D, Quondamatteo F, Herken R, Girolamo F, Marzullo A, Svelto M, Roncali L. 2003. Severe alterations of endothelial and glial cells in the blood-brain barrier of dystrophic mdx mice. Glia 42:235-251.

Nielsen S, Nagelhus EA, Amiry-Moghaddam M, Bourque C, Agre P, Ottersen OP. 1997. Specialized membrane domains for water transport in glial cells: high-resolution immunogold cytochemistry of aquaporin-4 in rat brain. J Neurosci 17:171-180.

Papadopoulos MC, Manley GT, Krishna S, Verkman AS. 2004. Aquaporin-4 facilitates reabsorption of excess fluid in vasogenic brain edema. FASEB J 18:1291-1293.

Papadopoulos MC, Verkman AS. 2005. Aquaporin-4 gene disruption in mice reduces brain swelling and mortality in pneumococcal meningitis. J Biol Chem 280:13906-13912.

Papadopoulos MC, Verkman AS. 2008. Potential utility of aquaporin modulators for therapy of brain disorders. Prog Brain Res 170:589-601.

Peters MF, Adams ME, Froehner SC. 1997. Differential association of syntrophin pairs with the dystrophin complex. J Cell Biol 138:81-93.

Pinheiro JC, Bates DM. 2000. Mixed-Effect models in S and S-PLUS. New York: Springer-Verlag.

Saadoun S, Papadopoulos MC, Davies DC, Krishna S, Bell BA. 2002. Aquaporin-4 expression is increased in oedematous human brain tumours. J Neurol Neurosurg Psychiatry 72:262-265.

Saadoun S, Tait MJ, Reza A, Davies DC, Bell BA, Verkman AS, Papadopoulos MC. 2009. AQP4 gene deletion in mice does not alter blood-brain barrier integrity or brain morphology. Neuroscience 161:764-772.

Taya K, Marmarou CR, Okuno K, Prieto R, Marmarou A. 2010. Effect of secondary insults upon aquaporin-4 water channels following experimental cortical contusion in rats. J Neurotrauma 27:229-239.

Thrane AS, Rappold PM, Fujita T, Torres A, Bekar LK, Takano T, Peng W, Wang F, Thrane VR, Enger R, Haj-Yasein NN, Skare O, Holen T, Klungland A, Ottersen OP, Nedergaard M, Nagelhus EA. 2011. Critical role of aquaporin-4 (AQP4) in astrocytic Ca2+ signaling events elicited by cerebral edema. Proc Natl Acad Sci U S A 108:846-851.

Vajda Z, Pedersen M, Fuchtbauer EM, Wertz K, Stodkilde-Jorgensen H, Sulyok E, Doczi T, Neely JD, Agre P, Frokiaer J, Nielsen S. 2002. Delayed onset of brain edema and mislocalization of aquaporin-4 in dystrophin-null transgenic mice. Proc Natl Acad Sci U S A 99:13131-13136.

Wen H, Nagelhus EA, Amiry-Moghaddam M, Agre P, Ottersen OP, Nielsen S. 1999. Ontogeny of water transport in rat brain: postnatal expression of the aquaporin-4 water channel. Eur J Neurosci 11:935-945.

Xu Q, Qaum T, Adamis AP. 2001. Sensitive blood-retinal barrier breakdown quantitation using Evans blue. Invest Ophthalmol Vis Sci 42:789-794.

Zeynalov E, Chen CH, Froehner SC, Adams ME, Ottersen OP, Amiry-Moghaddam M, Bhardwaj A. 2008. The perivascular pool of aquaporin-4 mediates the effect of osmotherapy in postischemic cerebral edema. Crit Care Med 36:2634-2640.

Zhou J, Kong H, Hua X, Xiao M, Ding J, Hu G. 2008. Altered blood-brain barrier integrity in adult aquaporin-4 knockout mice. Neuroreport 19:1-5.

FIGURE LEGENDS

Figure 1. Immunofluorescence micrographs showing the distribution of AQP4 and members of the DAPC in the parietal cortex of WT and *Aqp4*$^{-/-}$ mice. Co-immunostaining with antibodies against AQP4 **(A)** and GFAP **(B)** in WT reveals AQP4 immunoreactivity in astrocytes, with the most intense signal in perivascular endfeet (arrows; **C** is overlay). Double staining for AQP4 **(D)** and the microglial marker IBA1 **(E)** in WT (overlay in **F**). AQP4 immunofluorescence is not detectable in microglia (double arrowheads). Insets show a microglial cell at higher magnification. Arrows, perivascular astrocytic endfeet; asterisks, vessel lumen. In WT mice distinct immunofluorescence for α-syntrophin **(G)**, dystrophin **(H)**, and β-dystroglycan **(I)** was seen around cortical vessels of all calibers, including large penetrating vessels (crossed arrows) and capillaries (arrows; shown in higher magnification in insets). **Insets G-I,** Double staining with antibodies against the endothelial marker CD31 (blue) revealed that labeling for α-syntrophin, dystrophin , and β-dystroglycan (all red), was peripheral to the capillary endothelium (arrowheads), corresponding to perivascular astrocytic endfeet (arrows). **J-L,** Immunostaining in *Aqp4*$^{-/-}$ mice. α-Syntrophin immunofluorescence around capillaries was much weaker in *Aqp4*$^{-/-}$ mice **(J)** than in WT mice **(G).** Also for dystrophin the perivascular immunosignal was weaker in *Aqp4*$^{-/-}$ **(K)** than in WT mice **(H)**, whereas the β-dystroglycan labeling was indistinguishable between genotypes (compare **I** and **L**). Insets as in WT. Scale bars, A-F (including insets), 25 μm; G-L, 50 μm and 5 μm (insets).

Figure 2. AQP4 and α-syntrophin are mutually dependent upon each other for expression in perivascular astrocytic endfeet. **A-C,** Electron micrographs showing immunoreactivity for α-syntrophin in WT **(A)**, *Aqp4*$^{-/-}$ **(B)**, and *α-syn*$^{-/-}$ mice **(C)**. Note that α-syntrophin immunogold

labeling is associated with perivascular astrocytic endfoot membranes (arrowhead) in WT mice, and that the density of gold particles is lower in *Aqp4*$^{-/-}$ mice. Absence of labeling in *α-syn*$^{-/-}$ mice confirms selectivity of antibodies. **Insets in A-C,** Distribution of gold particles indicating α-syntrophin along an axis perpendicular to the perivascular astrocytic plasma membrane. The ordinate indicates number of gold particles per bin (bin width 4 nm). The abscissa indicates distance in nm from the midpoint (0 value) of the plasma membrane, cytoplasmic side negative. Note the distinct peak corresponding to the plasma membrane and its cytoplasmic vicinity in WT and *Aqp4*$^{-/-}$ mice, reflecting the localization of α-syntrophin. The gold particle density drops to background level ~50 nm from the midpoint of membrane, partly reflecting the size of the antibody bridge between the epitope and the corresponding gold particle. No peak is seen in *α-syn*$^{-/-}$ mice, in which the weak signal is non-specific. The total length of membrane sampled for WT, *Aqp4*$^{-/-}$ and *α-syn*$^{-/-}$ mice was 287 μm, 296 μm, and 188 μm, respectively. **D,** Quantitative analysis of immunogold reactivity for α-syntrophin and AQP4 along perivascular astrocytic endfoot membranes. Shown is α-syntrophin labeling of WT (74 profiles, 5 animals) and *Aqp4*$^{-/-}$ mice (74 profiles, 5 animals), and AQP4 labeling of WT (224 profiles, 7 animals) and *α-syn*$^{-/-}$ mice (243 profiles, 8 animals). Values represent mean number of gold particles per micrometer of membrane. Error bars are SEM, based on the sample after pooling the data from animals within each genotype. Values for α-syntrophin differed between WT and *Aqp4*$^{-/-}$ mice ($p<0.001$) and values for AQP4 differed between WT and *α-syn*$^{-/-}$ mice ($p<0.001$, mixed model statistical analysis, cf Materials and Methods). **E-F,** AQP4 labeling of perivascular astrocytic endfoot membranes (arrowhead) of WT mice **(E)** and *α-syn*$^{-/-}$ mice **(F)**. Insets show distribution of gold particles perpendicular to the membrane, as explained above. End, endothelial cells. Asterisks, perivascular endfeet. Scale bars, 0.2 μm.

Figure 3. *Aqp4* gene deletion does not alter ultrastuctural architecture of brain capillaries. Electron micrographs from WT **(A, B)** and *Aqp4*$^{-/-}$ mice **(C, D)** showed that the morphology of capillaries and perivascular astrocytes was indistinguishable between the genotypes. Notably, astrocytic endfeet (asterisks) did not appear swollen. Pericytes (P) and endothelial cell (End) tight junctions (arrowheads in insets) were present in both genotypes. Scale bars, 500 nm and 100 nm (insets).

Figure 4. Blood-brain barrier permeability and expression of endothelial tight junctional proteins are not affected by *Aqp4* gene deletion. HRP tracer is confined within the cortical vasculature in both WT **(A)** and *Aqp4*$^{-/-}$ **(B)** mice. Arrows denote capillaries shown at higher magnification in insets. Neither WT **(C)** nor *Aqp4*$^{-/-}$ **(D)** brains show extravasation of Evans blue albumin dye after systemic injection, nor do they differ significantly from each other in Evans blue content **(E)**. Values represent mean ± SEM. (**F**-**H**) Immunoblots of brain homogenates from 4 WT and 4 *Aqp4*$^{-/-}$ mice. The blots were probed for the endothelial tight junction proteins claudin-5 (**F**), occludin (**G**) and ZO-1 (**H**). Markers indicate molecular weight. Densitometric analysis revealed that the cerebral expression of claudin-5, occludin and ZO-1 in *Aqp4*$^{-/-}$ mice did not differ from that of WT (unpaired t-test, values are mean ± SEM). The signal was corrected for differences in protein loading by use of the density of actin staining.

AQP4
GFAP
AQP4 GFAP
A
B
C
AQP4
IBA1
AQP4 IBA1
D
E
F
α-syntrophin
dystrophin
β-dystroglycan
CD31
G
H
I
Wild-type
α-syntrophin
dystrophin
β-dystroglycan
CD31
J
K
L
Aqp4-/-

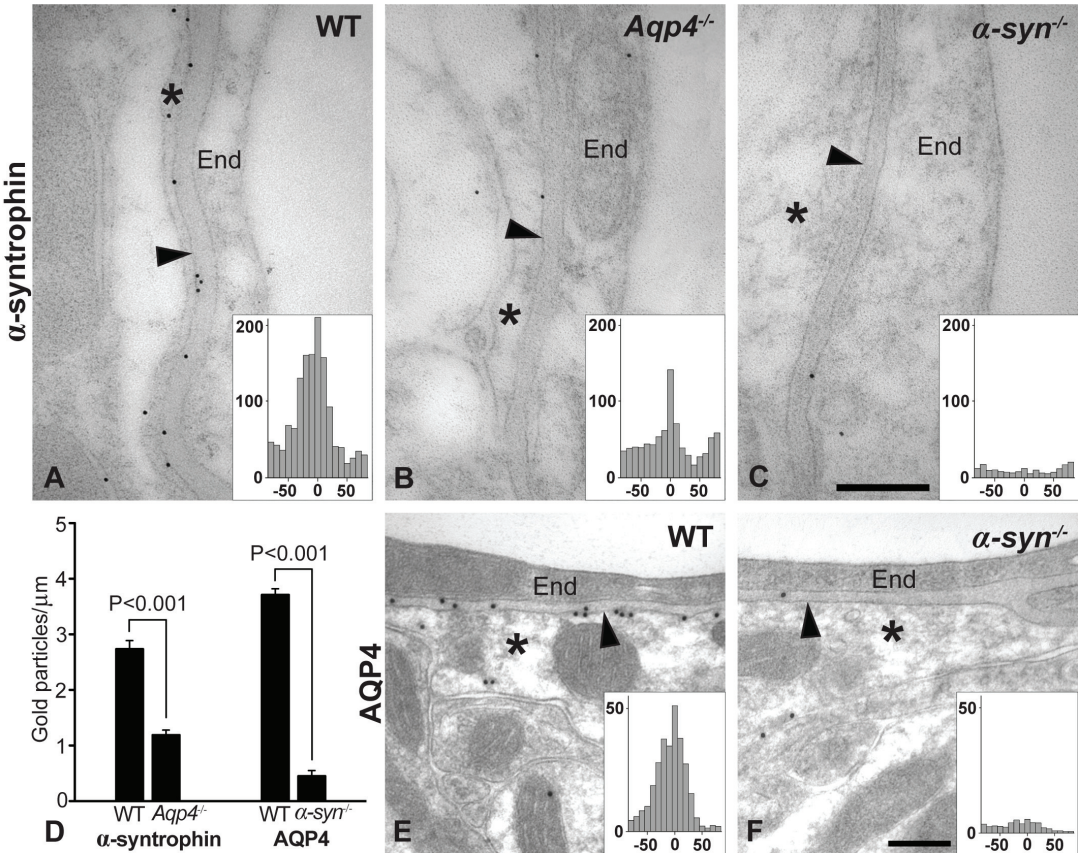
α-syntrophin
WT
Aqp4-/-
α-syn-/-
End
A
B
C
200
100
0
-50 0 50
D
Gold particles/µm
P<0.001
P<0.001
WT Aqp4-/-
α-syntrophin
WT α-syn-/-
AQP4
AQP4
E
F
50

Wild-type
Aqp4-/-
A
B
C
D
Lumen
P
End
*

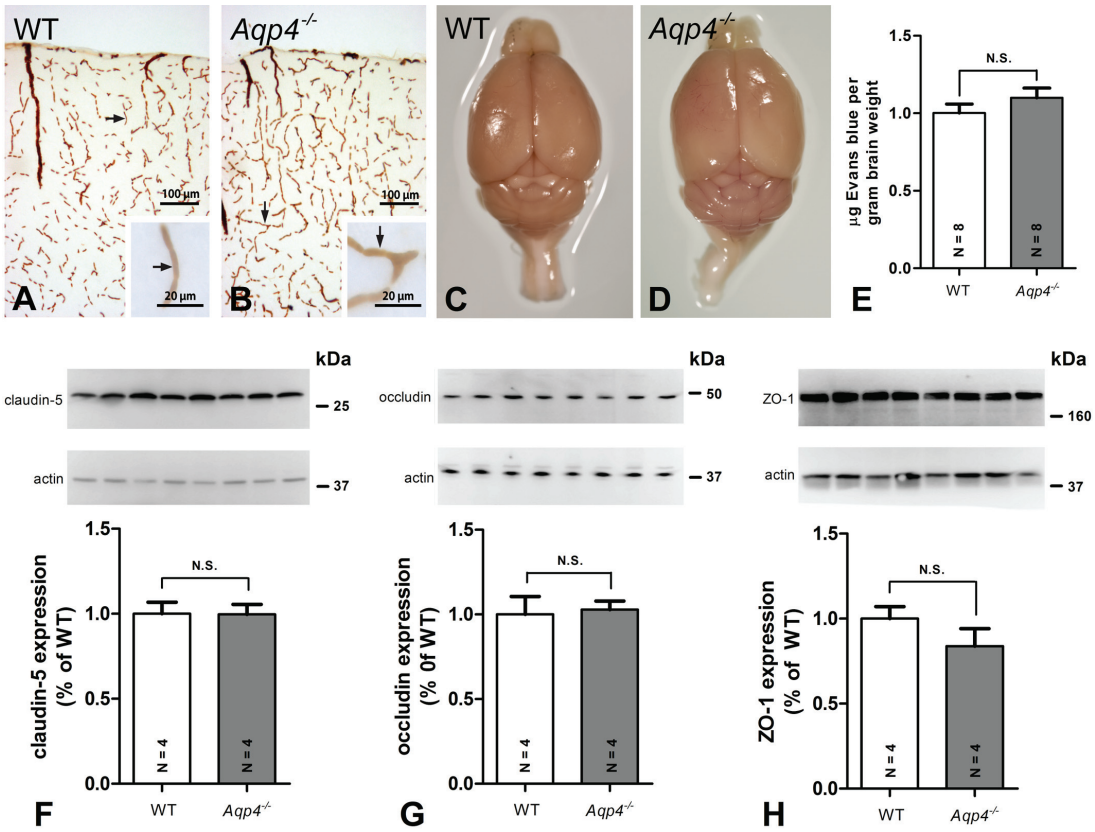
WT
Aqp4-/-
100 µm
20 µm
A
B
C
D
µg Evans blue per gram brain weight
N.S.
N = 8
E
kDa
claudin-5
25
actin
37
occludin
50
ZO-1
160
claudin-5 expression (% of WT)
occludin expression (% 0f WT)
ZO-1 expression (% of WT)
N = 4
F
G
H

IV

LIST OF ERRATA:

Page: 4 Paragraph: 2 Line :3
Was: go do also
Should be: also go to

Page: 4 Paragraph: 2 Line :7
Was: discussion
Should be: discussions

Page: 9 Paragraph: 3 Line :2
Was: Fig
Should be: Fig.

Page: 9 Paragraph: 3 Line :13
Was: transport cycle (MacAulay and Zeuthen 2010).
Should be: transport cycle (MacAulay and Zeuthen 2010). [moved text to the right; only layout was changed]

Page: 10 Paragraph: 4 Line :5
Was: AQP10-12
Should be: AQP10-12.

Page: 10 Paragraph: 4 Line :7
Was: (Badaut, Lasbennes et al. 2002; Gomes, Agasse et al. 2009; Ishibashi, Koike et al. 2009; Badaut 2010)
Should be: (Badaut, Lasbennes et al. 2002; Gomes, Agasse et al. 2009; Ishibashi, Koike et al. 2009; Badaut 2010).

Page: 14 Paragraph: 1 Line :3
Was: (Frigeri, Nicchia et al. 2001; Neely, Amiry-Moghaddam et al. 2001).
Should be: (Frigeri, Nicchia et al. 2001; Neely, Amiry-Moghaddam et al. 2001) (Fig.3).

Page: 22 Paragraph: 1 Line :5
Was: molecular function.
Should be: molecular function (Fig.5).